APPLICABILITY OF SYNTHETIC APERTURE RADAR FOR INVESTIGATING RIVER ICE BREAKUP ON THE KUPARUK RIVER, NORTHERN ALASKA

By

Angelica L. Floyd

RECOMMENDED:

Advisory Committee Co-Chair

Advisory Committee Co-Chair

Chair, Department of Geology and Geophysics

APPROVED:

Dean, College of Natural Science and Mathematics

Dean of the Graduate School

11/29/2012

Date

# APPLICABILITY OF SYNTHETIC APERTURE RADAR FOR INVESTIGATING RIVER ICE BREAKUP ON THE KUPARUK RIVER, NORTHERN ALASKA

A

THESIS

Presented to the Faculty

of the University of Alaska Fairbanks

in Partial Fulfillment of the Requirements

for the Degree of

MASTER OF SCIENCE

By

Angelica L Floyd, B.S.

Fairbanks, Alaska

December 2012

## Abstract

A combined use of remote sensing techniques and field measurements is a pragmatic approach to study Arctic hydrology, given the vastness, complexity, and logistical challenges posed by most Arctic watersheds. This study investigates the use of synthetic aperture radar (SAR) to define spring breakup of the Kuparuk River on the North Slope of Alaska. A time series (years 2001-2010) of SAR images was assembled at the river mouth on the Arctic Coastal Plain. A statistical analysis was used and was limited to three variables: image brightness, variance in brightness over the river length, and a rank order analysis accomplished by segmenting the river and ranking segments in order of relative brightness. Variance was the only reliable breakup indicator of the three tested. A shorter one year temporal stack was assembled at the river's headwaters for a visual interpretation, which had limited success. Results from both analyses were calibrated with in-situ stream gauge data. River ice breakup is a highly complex process which may be defined differently by the remote sensing community and hydrologists, due to the sensitive nature of SAR, which may indicate surficial changes on the river before any discharge is recorded.

## Table of Contents

Page

## List of Figures

Page

## List of Tables

Page

## List of Appendices

Page

## List of Acronyms

| | |
|---|---|
| ASF | Alaska Satellite Facility |
| cfs | Cubic feet per second |
| dB | Decibel |
| DEM | Digital Elevation Model |
| ERS-2 | European Remote Sensing Satellite |
| FFT | Fast Fourier Transform |
| NOAA | National Oceanic and Atmospheric Administration |
| SAR | Synthetic Aperture Radar |
| SROC | Sum of Rank Order Change |
| USGS | United States Geological Survey |
| WERC | Water and Environmental Research Center |

## Acknowledgements

I would like to thank and acknowledge the support and encouragement I received from many people and organizations throughout my graduate studies.

I am greatly appreciative of my exceptional graduate committee members: Drs. Anupma Prakash, Anna Liljedahl, Franz Meyer, and Rudi Gens. They all went above and beyond to ensure my successful completion of this research and I have benefited from their guidance and instruction. It was a privilege to work with each of them. My advisor, Dr. Anupma Prakash, deserves special thanks for the kindness and care she showed me during the past several years, as well as her untiring efforts and attention to my work. I am extraordinarily fortunate to have worked with her.

I would like to thank my funding agencies, the Department of Geology and Geophysics, Alaska Satellite Facility, Alaska EPSCoR Program (grant number G00004248), Geophysical Institute, Water and Environmental Research Center, Alaska Climate Science Center, and Scott Rupp at Scenarios Network for Alaska & Arctic Planning.

I would also like to thank Joel Homan for installing a time lapse camera in the field on my behalf. Lastly, a big thanks to my many friends and colleagues at UAF who have made it such a pleasure to work here every day.

## 1.0 Introduction

### 1.1 Background and Motivation

Arctic rivers affect global climate. Not only do these rivers control freshwater export into the Arctic Ocean, they also influence sediment transport, oceanic processes, and sea ice. The freshwater export from the Arctic region, which has increased from the large Eurasian rivers (Peterson *et al.,* 2002), is estimated to represent 10% of global runoff (Steele *et al*., 1996). While the hydrology of the Arctic clearly has a large impact globally, this region is largely remote. The logistical challenges involved in Arctic research have hindered the scientific community's understanding of the role this landscape has on the global climate system.

River ice breakup has an important effect on sea ice and oceanic processes. Shorefast ice can be rapidly eroded by river runoff in the spring. Changes to the timing or volume of river discharge can affect the extent of the ice cover (Searcy *et al*., 1996), and therefore, regional land-atmosphere energy exchanges. In addition to its influence on sea ice, much of the freshwater drains into the Atlantic Ocean where it contributes to the formation of North Atlantic Deep Water (NADW) (Rahmstorf, 2002), which is a significant factor in global climate. Between the 1940s and today, winter air temperatures have increased in Siberia, resulting in greater precipitation and a marked increase in river discharge (Savelieva *et al.,* 2000; Yang *et al*., 2002; Berezovskaya *et al*., 2004). There is a concern that if Arctic freshwater discharge increases drastically, it may affect NADW formation and alter the thermohaline circulation of the world's oceans (Broecker, 1997; Peterson *et al.,* 2002). These factors make a compelling case to focus research efforts on understanding Arctic river processes. One way to better comprehend river response in remote locations of the Arctic is to use remote sensing tools.

One of the unique traits of Arctic rivers is the extreme seasonality of flow. During the long winter months the channels are frozen and limited, if any, discharge occurs (Kane *et al.*, 1991). Spring runoff is the major hydrologic event of the year, as a snowpack that has accumulated for eight to nine months rapidly melts (Kane *et* al., 1997; Kane *et* al., 2000; Kane *et al.*, 2003). The ablation period typically lasts from seven to fourteen days (Kane *et al*., 1997). McNamara *et al*. (1998) found that snowmelt provides up to 80% of the annual runoff from the Kuparuk River, Northern Alaska. Summer precipitation is critical in thawed season river response (Kane *et al*., 2003; Kane *et al*., 2008). Spring and summer flows are therefore mainly responsible for the geomorphic changes of the river channel (Delaney *et al*., 1990).

The combination of the abrupt snowmelt on the surrounding tundra and the thick river ice can result in dramatic flooding events. Ice jams are often related to these flood events. Ice jams occur when river ice has been broken into large chunks and obstructs parts of the river channel, effectively damming the river until the ice jam breaks. Ice jams are frequently unpredictable (Martini *et al.,* 1993) and can be highly destructive to anything in their path. Ice jams and the associated flooding left in their aftermath are of great consequence to both Northern communities, as well as oil and gas companies operating in the Arctic. Understanding the timing of river ice breakup can help to mitigate hazards related to large flood events.

This research is designed to address the challenge of studying remote Arctic rivers. Few rivers in the Arctic have been gauged and even fewer are actively measured (Bring and Destouni, 2009) Satellite imagery can potentially allow for a pan-Arctic perspective of the major hydrologic event

in remote Arctic rivers. This study aims to develop a methodology for determining when an Arctic river undergoes its annual breakup flood, so that the knowledge may be exported for use on other rivers in the region.

### 1.2 Hypotheses

This study centers on two primary hypotheses listed below.

1. Information from statistical analysis of Synthetic Aperture Radar (SAR) image data can be used to bracket breakup timing of a relatively large (>8,000 $km^2$), braided Arctic river, such as the lower portion of the Kuparuk River, North Slope, Alaska.
2. The onset of breakup can be captured in a small (<200 $km^2$) single channel river through a visually distinct change in signature on SAR images, such as the upper portion of the Kuparuk River, North Slope, Alaska.

### 1.3 Goal and Objectives

The overarching goal of this research was to use SAR images from May through July to identify breakup in a decadal time series (2001-2010) for parts of the Kuparuk River. To meet this general goal the specific objectives were:

- Investigate for confounding image statistics caused by factors such as wind velocity or ice types that may limit/influence the usefulness of SAR data for the analysis of river breakup timing.
- Bracket breakup initiation in Lower Kuparuk River by a statistical analysis of SAR data guided by field data.

- Visually bracket breakup initiation in Upper Kuparuk River guided by field data, as limitations in spatial resolution prohibit a meaningful statistical analysis.
- Summarize the advantages and limitations of SAR for investigating breakup in both braided and unbraided reaches of a selected Arctic river.

The thesis is organized into six chapters. Chapter 1 (this chapter) presents the background on Arctic hydrology and the motivation for this study along with the hypotheses, goals, and objectives of this research. Chapter 2 introduces the study area including its geological and hydrological setting. Chapter 3 provides details on the data sets used, outlines the workflow, and explains the methods used to meet the research objectives. Results and discussions are presented in Chapter 4. Chapter 5 provides conclusions, advantages, and limitations of the study along with recommendations for future work.

## 2.0 Study Area

### 2.1 General Description

#### 2.1.1 Location

For this research, two study area locations were selected on the Kuparuk River on the Alaska North Slope (Figure 2.1). The Upper Kuparuk River study area shown in Figure 2.2 is bounded by latitudes 68° 55' 19" N and 68° 43' 57" N, and longitudes 149° 33' 1" W and 149° 41' 37" W. The Lower Kuparuk River study area, depicted in Figure 2.3, is bounded by latitudes 70° 25' 7" N and 70° 14' 1" N and longitudes 148° 59" 16' W and 149° 1' 11" W.

Unlike most Northern Alaska rivers, the Kuparuk River has two working gauging stations that are monitored regularly. The first station was established by the USGS in 1973 at the Lower Kuparuk River (station ID 15896000) and the second by the Water and Environmental Research Center (WERC) at UAF in 1985 on the Upper Kuparuk River. The station monitored by WERC is located in the foothills of the Brooks Range, while the USGS station is located on the coastal plain. The Kuparuk River is well studied by several research groups and a large body of published literature is readily available on the climatic setting, hydrology, and history of this river (McNamara *et al.*, 1998; Muller *et al.*, 1998; Kane *et al.* 1991, Kane *et al.,* 1997; Kane *et al.*, 1998; Kane *et al.*, 2000; Kane *et al.,* 2003; Hinzman *et al.*, 2008).

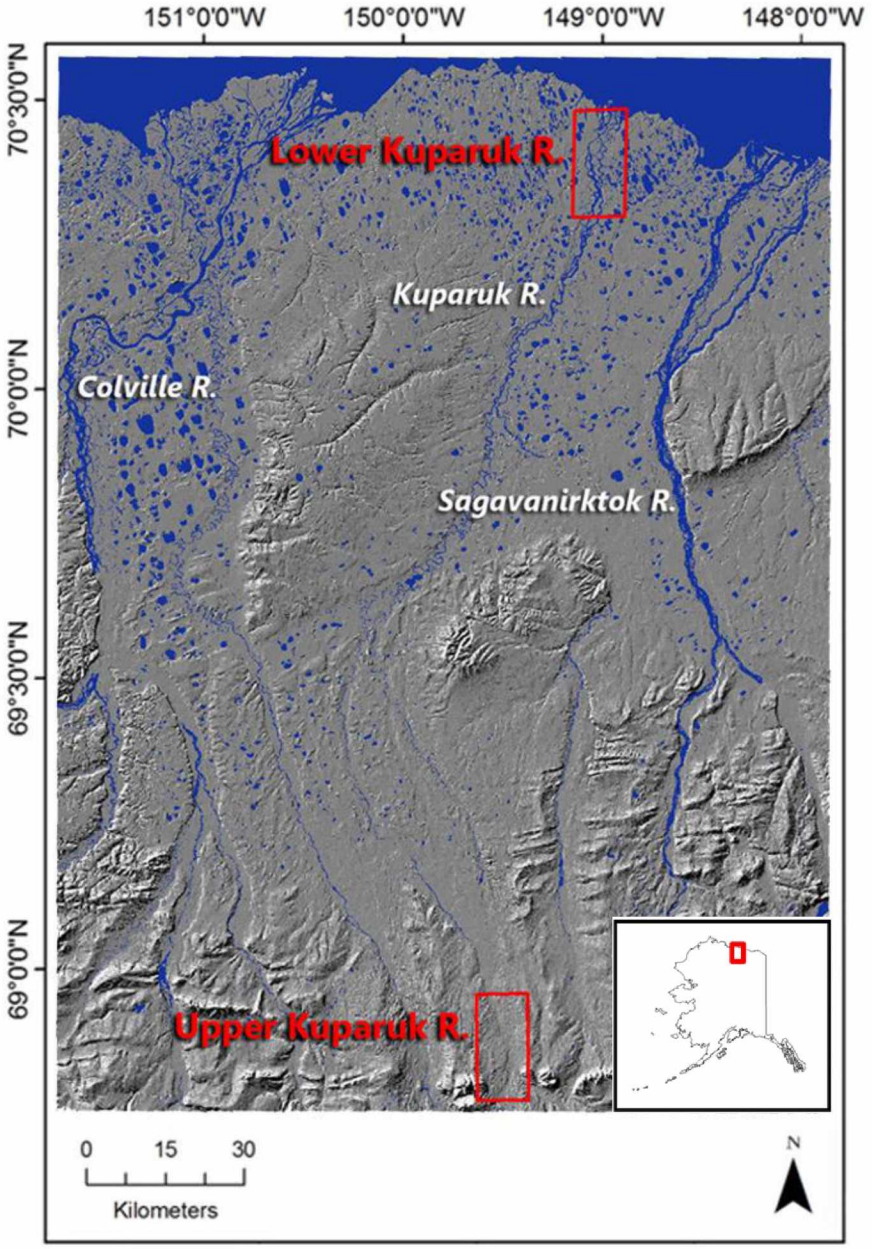


Figure 2.1: General study area map showing extents of the two selected sites: Upper Kuparuk River and Lower Kuparuk River. The topography of the region is shown as a shaded relief and the neighboring Colville and Sagavanirktok watersheds are labeled. An inset of the Alaska map is also shown.

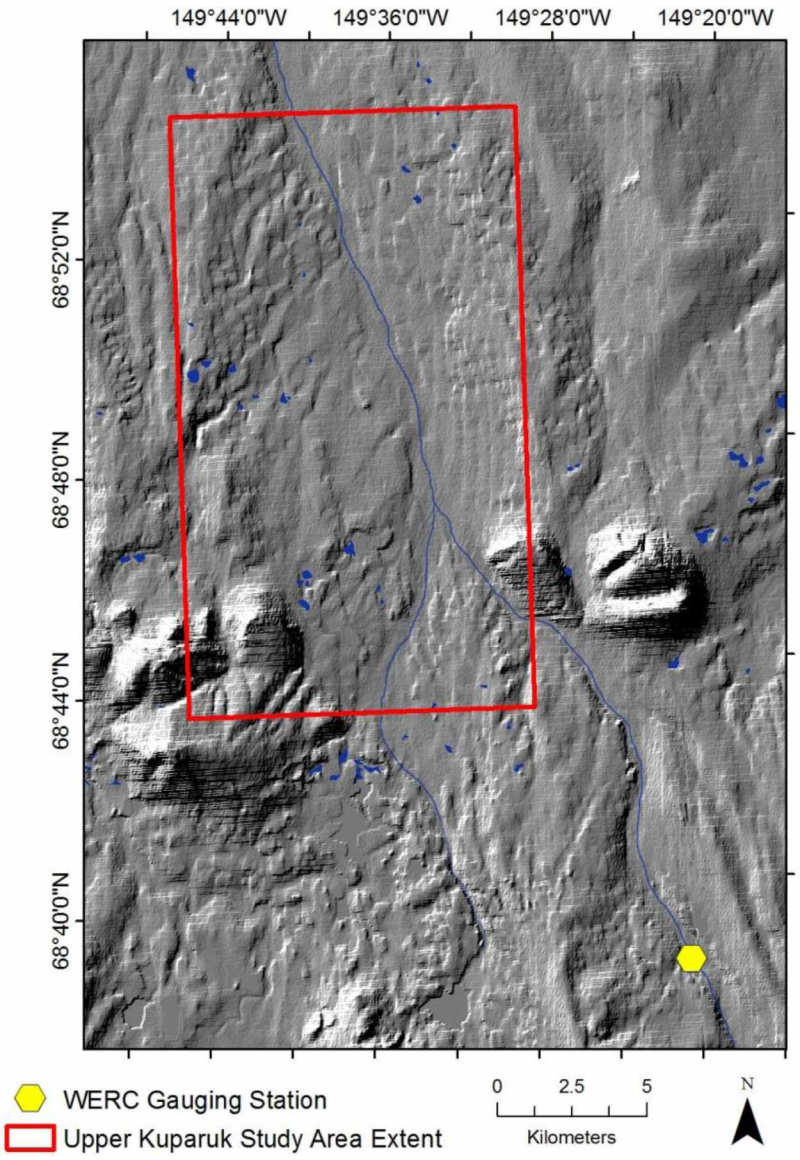


Figure 2.2: Upper Kuparuk River study area. The WERC gauging station is shown about 13 km upstream of the Southern end of the study area extent. The terrain is increasingly hilly south towards the Brooks Range.

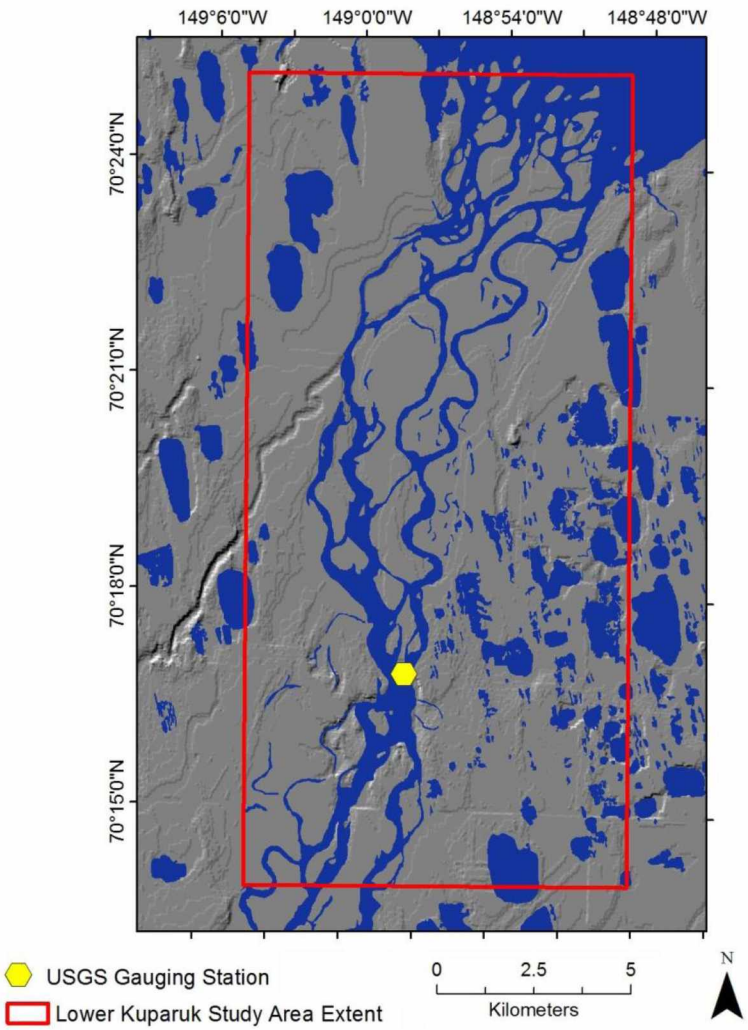


Figure 2.3: Lower Kuparuk River study area. The location of the USGS Lower Kuparuk River gauging station (USGS ID number 15896000) is marked.

### 2.1.2 Geomorphology

The Kuparuk River watershed drains 8,140 km$^2$ in a north trending basin nearly 250 km in length (Kane *et al.*, 2000), from the northern foothills of the Brooks Range to the Arctic Ocean. The average elevation of the Kuparuk River basin, over its complete length, is 245 m (McNamara *et al.,* 1998). Though some North Slope rivers do have a contribution from glacial meltwater, the

Kuparuk River basin is unglaciated. The entire watershed is underlain with continuous permafrost, with a depth near 250 m at the headwaters to over 600 m on the coastal plain (Osterkamp and Payne, 1981). There are also a number of aufeis fields along the length of the Kuparuk watershed suggesting ground water recharge at some locations (Yoshikawa *et al.,* 2007).

The Upper Kuparuk River heads in the foothills of the Brooks Range where it is a single channel stream with a cobble bed, which is fed by spring snowmelt and frequent summer storms. The ground is boggy and waterlogged in summer and tussock sedge tundra is the primary vegetation. Drainage features called hillslope water tracks are abundant in the Upper Kuparuk watershed (Hastings *et al.,* 1989; Kane *et al.,* 1991; Trochim *et al*., 2010a; Walker *et al.,* 1989). Water tracks are linear or curvilinear belts of increased soil moisture that serve as runoff pathways and transport water from higher elevations to the river basin (McNamara *et al*., 1999; Trochim *et al*., 2010b). A field photo of the Upper Kuparuk River near the study site for this research is shown in Figure 2.4.

Figure 2.4: Photo of the Upper Kuparuk River near the Dalton Highway, May 24, 2005. Photo credit A. Liljedahl.

Downstream the Kuparuk River widens as it flows across the tundra and coastal plain and transitions from a single channel river to a braided river. The topography is flat near the coast and dotted with many lakes, which increase in frequency closer to the coast (Shiklomanov and Nelson, 2002), as is evident in Figures 2.1 and 2.2. The vegetation is shrublands and wet tussock tundra; 83% of the coastal plain is categorized as wetlands resulting in a large capacity of surficial storage (Kane *et al.,* 2000). This region has been developed for oil and gas exploration after the discovery of crude oil in the nearby Prudhoe Bay oil field. The Kuparuk oil field

underlies the present day Kuparuk River and drilling pads and other industry infrastructure have been installed on both sides of the river.

### 2.1.3 Hydro-climatology

Climate varies between the headwaters and the river mouth of the Kuparuk. The coastal plain witnesses cold winters, and cool summers with wind from the Arctic Ocean. The Upper Kuparuk River sees a greater annual temperature variation than the coastal plain as an effect of the continental summer climate, but fluctuations exist depending on elevation (Nelson *et al.,* 1997). Mean annual air temperature at the Lower Kuparuk River is about -12°C, with temperatures only rising above freezing from June to September. Precipitation measurements vary based on location and the collection device employed, but range between 140 mm/year (Nelson *et al.,* 1997) and 292 mm/year (Déry *et al.,* 2005) at the Upper Kuparuk River. Annual precipitation at the Lower Kuparuk River averages 173 mm (Liljedahl *et al.*, 2011), but tends to be greatest in July and August (Rovansek *et al*., 1996). The entire watershed is snow covered between seven and nine months of the year and the majority of the precipitation falls as snow (Kane *et al.*, 1997). At the Upper Kuparuk River approximately 40% of precipitation falls as snow and this number increases to about 50% at the Lower Kuparuk River (Zhang *et al.*, 1996). Runoff typically begins in mid to late May at the Upper Kuparuk River and late May to early June at the Lower Kuparuk River; freeze-up often begins between mid to late-September and early October (Best *et al.,* 2005). Vegetation, soil moisture, and depth of the active layer vary along the river's length (Shiklomanov and Nelson, 2002).

### 2.1.4 Geologic Setting of the North Slope

The geology of the North Slope is complicated and not fully understood, but has been divided into four primary sequences as derived from Hubbard *et al.* (1987). From oldest to youngest these are the Franklinian, Ellesmerian, Beaufortian, and Brookian. The following summary of North Slope geologic history is based on Hubbard *et al.* (1987).

The earliest known sequence in this region is the Franklinian (Early Devonian) dating back 400 million years. The Franklinian is marked by formation of a stable continental platform composed of metamorphosed sandstones, carbonates, and local granites and volcanics. This period ended with a mountain building event that greatly deformed and altered the rocks which quickly eroded away into a low-lying coastal plain.

The Ellesmerian sequence (Mid/Late Devonian through Triassic) is of great economic interest because the primary petroleum and reservoir source rocks at Prudhoe Bay were deposited during the Upper Ellesmerian. The Lower Ellesmerian was characterized by south facing passive margin deposition as clastic sediments from the landmass oriented north of the modern Beaufort Sea coast eroded into the Arctic Alaska Basin. The Middle and Upper Ellesmerian depict a series of transgressive/regressive events and deposition of mainly shales, and carbonates in the Middle Ellesmerian and a heterogeneous assemblage of fine to coarse-grained siliciclastic rocks, organic-rich shales, and carbonates in the Upper Ellesmerian.

The Beaufortian sequence (Early/Mid-Jurassic to Early Cretaceous) was dominated by extensional processes and rifting. Failed rifting in the Upper Triassic led to the formation of the

Barrow Arch. Throughout the Lower and Middle Cretaceous the Barrow Arch began a counterclockwise rotation and subsequent rifting from Arctic Canada. The southern edge of the Arch sloped southward and eroded sediments filled this basin where they were later buried beneath the Colville foreland basin of the Brooks Range.

The Brookian sequence is the most recent and dates from Late Jurassic to Early Cretaceous and is notable for the formation of the Colville Basin, which the present-day Kuparuk River is eroding into. During the Brookian the formerly south facing margin became north facing. Crustal shortening produced three distinct phases of mountain building during this time, leading to the rise of the Brooks Range. Depositional environments suggest a progressive shallowing of the Colville Basin as sediments from the Brooks Range gradually filled it. The Lower Brookian sequence is made up of turbidites, conglomerates, shales, coal, and lithic sands. The Middle Brookian is notable for the formation of the Colville Group and is made up of shales, silts, sandstones, mudstones, conglomerates, and coals. This suggests deposition in a prograding shallow marine and deltaic environment. The Upper Brookian consists of mudstones and sandstones from deltaic systems. Quaternary deposits consist of sand and gravel from eroded Brookian sediments. Numerous Eolian sand dunes are a remnant of cold, dry, Ice Age conditions.

The geomorphology, climate and geologic setting of this region all control the hydrology of the watershed, which is described in Section 2.2.

## 2.2 Hydrologic Setting

### 2.2.1 Arctic River Breakup Processes

The type of river breakup can vary from year to year with two possible extremes emerging: thermal and mechanical breakup (Martini *et al.,* 1993). A thermal breakup occurs when most of the ice that is attached to the banks simply melts in place (Ferrick and Mulherin, 1989). The thermal breakup is an extended process supported by a slowly increasing air temperature. In these instances, peak discharge remains relatively low compared to a mechanical breakup, and ice jams are weak if they even occur at all (Niehus, 2002; Beltaos, 2003). The second pattern, known as mechanical breakup, represents rapid and dramatic breakup. Here, rapid increase in air temperature melts the snow on the surrounding landscape that floods the ice filled river channels. The dramatic influx of water creates stresses in the river ice that lead to fractures. The river ice is lifted from the bed and banks and broken into chunks that move downstream (Niehus, 2002; Beltaos, 2003). Damages to infrastructure from ice jams, ice drives and ice floes are common. Ice floes can easily move over the river banks onto the floodplains (Ferrick and Mulherin, 1989; Martini *et al.,* 1993). A combination of thermal and mechanical breakup is most common. Generally, some amount of melting occurs which increases discharge and fractures the ice cover to some degree (Beltaos, 2003).

Research has shown that the breakup pattern and magnitude of ice jams cannot be reliably predicted, even though the approximate time of the flood can be easily estimated (Zachrisson, 1988; Martini *et al.,* 1993). Beltaos (2003) proposed a physics-based threshold to delineate between thermal and mechanical breakup, but requires numerous field-based measurements that are impractical in a remote location such as the Arctic. An example image of late-stage

mechanical breakup from the Kuparuk River in early June 2012 is shown in Figure 2.5; small ice chunks can be seen moving downstream.

Figure 2.5: Ice chunks moving downriver on the Lower Kuparuk River, June 1, 2012.

### 2.2.2 River Ice Types

River ice formation is a complicated process. Several types of ice can form on rivers during the winter season. Four types are described here, based on a case study of the Albany River in Ontario from Martini *et al.* (1993): black ice, snow slush ice, frazil ice, and anchor ice. However, there are additional ice types that can form from variants or combinations of these four. Black ice forms from freezing river water (Michel, 1978). The upper part of any ice-cover is a mixture of snow and flood water called snow slush ice; larger wind-blown particles and flood material such as vegetation is also found in this top layer (Michel and Ramseier, 1971; Gerard, 1983).

In conditions when the water is supercooled frazil ice can form, which is an aggregation of ice particles that freeze together (Michel and Ramseier, 1971; Williams and Mackay, 1973; Ashton, 1980; Ashton, 1986; Tsang, 1982). Frazil initially forms in areas of the river that are moving, such as the thalweg, where the flow is most turbulent and the formation of black ice is impeded by the motion of the water. Additionally, frazil contains many air bubbles and has a whitish appearance with a rough surface (Martini *et al.,* 1993). Anchor ice is frazil that attaches to the stream bottom (Michel and Ramseier, 1971; Smith, 1980; Tsang, 1982; Gerard, 1983; Ashton, 1986). The stream bottom, notably pebbles if it is a gravel bed, tend to be colder than the surrounding water, thus ice attaches there. Anchor ice can rip these pebbles from the bed if it is thick enough to float and the buoyancy of the ice overcomes the mass of the attached sediment (Osterkamp, 1975). A ground penetrating radar (GPR) study undertaken by Best *et al.* (2005) found that while much of the Upper Kuparuk River freezes to the bed during the winter months, portions of the Lower Kuparuk River do not.

These different ice types play a role in how ice is recognized and can be interpreted in SAR imagery. The backscatter of clear ice with no inclusions is different than ice that has numerous air bubbles or sediments trapped inside. Depending on the signal wavelength of a microwave remote sensing system, impurities in the ice matrix can cause volume scattering, of which air inclusions within the ice are the primary source (Michel and Drouin, 1972; Mermoz *et al.,* 2008). These small differences in backscatter can help identify different ice types on a river that is wide compared to the resolution of the observing remote sensing system. However, at a 12.5 meter resolution the Kuparuk River is too narrow to rely on satellite remote sensing methods to

classify ice types. Multiple ice types may be present within a single pixel and overlap each other, leading to a confounding array of backscatter values.

## 3.0 Data and Methods

### 3.1 How SAR Works

Synthetic Aperture Radar (SAR) is an active remote sensing technique where the sensor emits a microwave pulse, which travels to the ground and is backscattered. The amount of returned energy can be described by the direction of this backscatter. Bright areas in the focused image indicate microwaves scattered back towards the sensor and dark areas indicate microwaves scattered away from the sensor. As can be seen in Figure 3.1, signals are recorded along the flight path, or azimuth direction, perpendicular to the flight direction, or range direction. The brightness determines how much of the signal is received while the flight time of the signal influences where it is located in the image after processing.

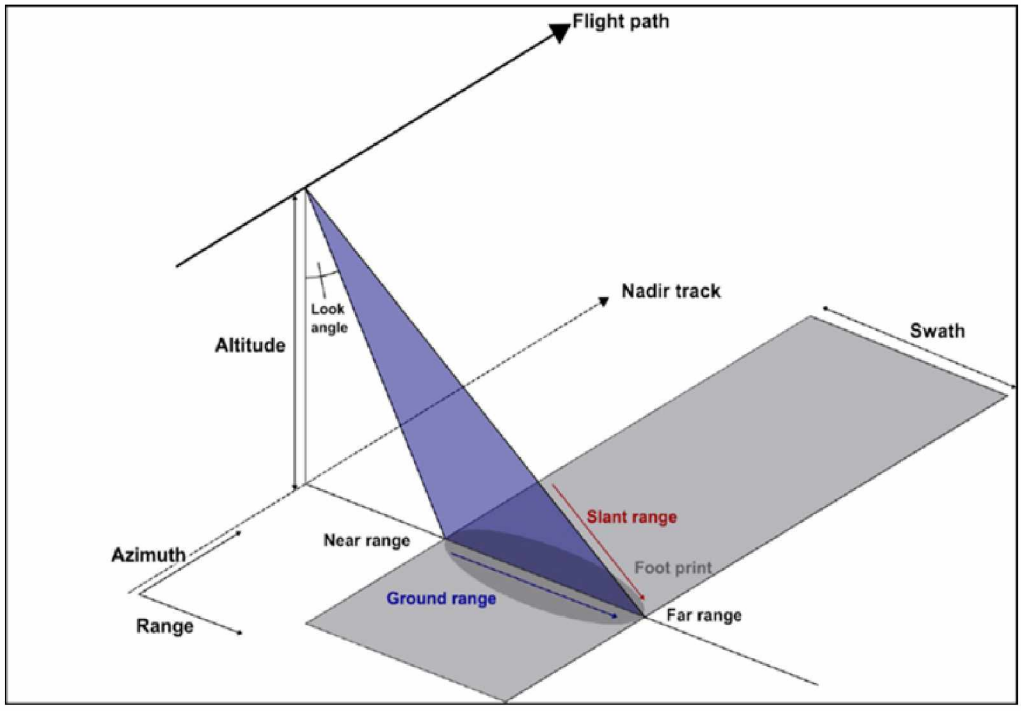


Figure 3.1: SAR satellite geometry. Diagram showing the satellite's right-looking orientation and viewing geometry. The swath is the ground area illuminated during image acquisition (Gens, 2008).

Due to the side-looking geometry, SAR is subject to several geometric distortions that require preprocessing to mitigate: the related effects of layover, foreshortening and shadows. Before these complications can be discussed, the viewing geometry of the system must be understood. The area of the ground being illuminated by the sensor is called the swath. The look angle is the angle between nadir and the antenna pointing direction. The change in look angle across the swath leads to the unwanted effects of layover and foreshortening, illustrated in Figure 3.2 (Hanssen, 2001; Lillesand *et al*., 2008; Woodhouse, 2006). These occur most often and most strongly in areas with substantial changes in topography such as mountainous or hilly regions. If the microwave pulse hits the top of the mountain prior to the base, the sensor images the landscape as if the top of the mountain was closer to the sensor than the bottom of the mountain. This often appears as though mountains are laying over on their sides, hence the name layover. A less severe form of this effect is foreshortening where the microwave pulse hits the side of the mountain first, or is scattered by both the top and bottom simultaneously. While foreshortening does not cause the topography to appear toppled over, it does compress sides of topographical features facing the sensor. A third problem related to both layover and foreshortening is shadows. In cases where topography completely blocks microwaves from

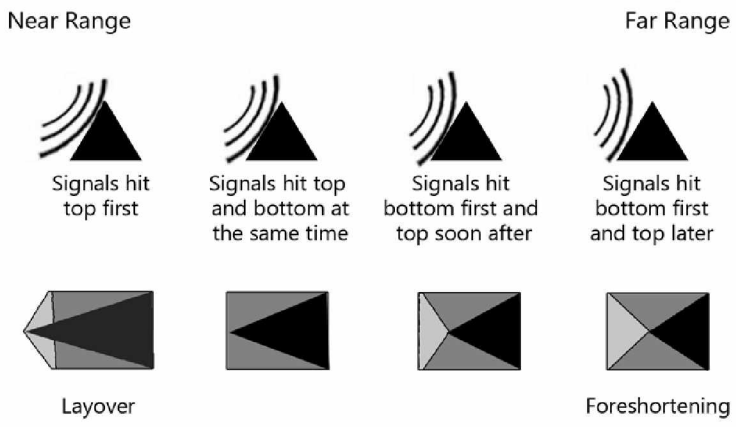


Figure 3.2: Schematic of layover and foreshortening effects in SAR images. Modified from the original in Lillesand *et al.* (2008).

imaging the sides farthest from the sensor, shadows develop. It is not possible to correct for shadows because information in those regions is absent (Hanssen, 2001; Lillesand *et al.*, 2008; Woodhouse, 2006).

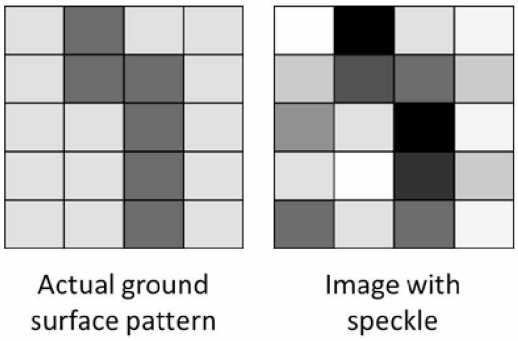


Figure 3.3: Example of how speckle results in a grainy image appearance. Figure modified from original in Lillesand *et al.* (2008).

Often confused with noise, speckle is a side effect of the radar imaging system that gives SAR imagery its characteristic grainy appearance. An example of speckle can be seen in Figure 3.3. When the sensor emits a narrow-band coherent microwave pulse, all the waves are in phase. As these waves travel to the ground and are scattered they become out of phase with one another. Some waves scatter multiple times before returning to the sensor and the image intensity in a pixel is then formed from a weighted sum of the various backscatter contributions. Speckle is a result of interference among the coherent echoes of the individual scatter vectors in one resolution cell. Unlike noise, which is random, speckle can theoretically be reproduced in subsequent satellite passes of the same region if the viewing geometry and surface conditions are exactly the same each time. Speckle can never be entirely removed from an image but it can be lessened through a processing step called multi-looking (Hanssen, 2001).

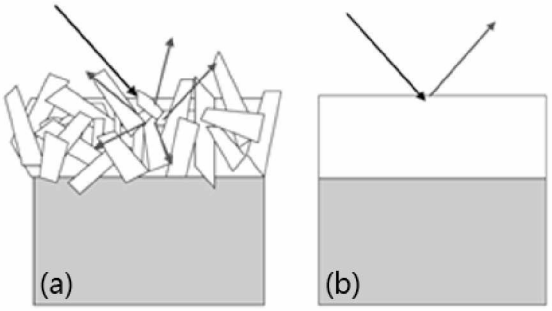


Figure 3.4: Interaction between SAR and ice. Diagram (a) represents rough, wet ice, which backscatters many incoming microwaves. Diagram (b) represents smooth, wet ice serving as a specular reflector. Illustration is taken from Unterschultz *et al.* (2009).

Smooth open water surfaces act as specular reflectors which scatter microwaves away from the sensor so little backscatter is returned. This causes open water to have a dark appearance in SAR images (Weber *et al.*, 2003). Ice can give both a bright and dark response in SAR depending on the surface smoothness, as depicted in Figure 3.4. If the ice surface is wet and rough diffuse scattering occurs and the ice surface will look relatively bright in the SAR image. If the ice is smooth and wet (possibly from saturated snow or meltwater on the surface) it behaves as a specular reflector, similarly to open water, and looks dark on the SAR image (Unterschultz *et al.*, 2009). Volume scattering occurs when the snow and/or ice layer is dry and microwaves penetrate the surface only to be scattered by discontinuities within the ice matrix such as cracks, air bubbles, sediment, and pockets of liquid water. Volume scattering can lead to significant backscatter depending on how inhomogeneous the ice package is (Unterschultz *et al.*, 2009). If ice is frozen to the ground, backscatter is influenced by the changes in material properties between ice and rock, though this river likely does not freeze to the channel (Best *et al.*, 2005).

## 3.2 Data Sources

### 3.2.1 Remote Sensing Data

This analysis utilizes a large dataset encompassing a ten year time span. SAR images from 2000-2010 (data from the year 2000 were later removed from the analysis due to low temporal

resolution) were collected from the Alaska Satellite Facility's RADARSAT-1 and ERS-2 archives. Both sensors are singularly polarized, RADARSAT-1 in HH polarization and ERS-2 in VV, and both sensors operate in the C band with microwave wavelengths of approximately 5.6 cm and 5.3 cm, respectively. Processed images from both sensors have 12.5 meter square pixels.

Information pertinent to the SAR images was recorded in a spreadsheet. This included the full granule name, look angle, time and date of image acquisition, and a notation of whether the satellite pass was acquired in an ascending or descending mode. The spreadsheet was organized by year, with a separate worksheet for each year. Later, meteorological information such as wind speed and temperature were added.

Table 3.1: List of the 65 SAR granules used for analysis of the Lower Kuparuk River. Granule name and date of satellite acquisition are listed. The prefix E2 refers to the ERS-2 satellite and R1 means the granule is from the RADARSAT-1 satellite.

| Granule | Date | | Granule | Date |
|---|---|---|---|---|
| R1_29057_ST2_F273 | 5/29/01 | | E2_58285_STD_F273 | 6/13/06 |
| E2_31961_STD_F273 | 5/31/01 | | E2_58557_STD_F273 | 7/2/06 |
| R1_29249_ST3_F177 | 6/12/01 | | E2_58786_STD_F273 | 7/18/06 |
| E2_32276_STD_F272 | 6/22/01 | | E2_58829_STD_F272 | 7/21/06 |
| E2_32462_STD_F273 | 7/5/01 | | E2_63072_STD_F177 | 5/14/07 |
| E2_36785_STD_F273 | 5/3/02 | | E2_63295_STD_F273 | 5/29/07 |
| E2_37292_STD_F177 | 6/8/02 | | E2_63338_STD_F273 | 6/1/07 |
| E2_37515_STD_F273 | 6/23/02 | | R1_60462_ST3_F176 | 6/5/07 |
| E2_37744_STD_F273 | 7/9/02 | | E2_63530_STD_F177 | 6/15/07 |
| E2_42024_STD_F273 | 5/4/03 | | E2_63573_STD_F177 | 6/18/07 |
| E2_42030_STD_F177 | 5/5/03 | | R1_60719_ST1_F177 | 6/23/07 |
| E2_42488_STD_F177 | 6/6/03 | | E2_63796_STD_F274 | 7/3/07 |
| E2_42525_STD_F273 | 6/8/03 | | E2_68305_STD_F273 | 5/13/08 |
| E2_42797_STD_F273 | 6/27/03 | | E2_68311_STD_F177 | 5/14/08 |
| E2_47306_STD_F273 | 5/7/04 | | E2_68348_STD_F273 | 5/16/08 |
| E2_47498_STD_F177 | 5/21/04 | | E2_68583_STD_F177 | 6/2/08 |
| E2_47764_STD_F273 | 6/8/04 | | E2_68806_STD_F273 | 6/17/08 |
| E2_47999_STD_F177 | 6/25/04 | | E2_68812_STD_F177 | 6/18/08 |
| E2_48036_STD_F273 | 6/27/04 | | E2_68849_STD_F273 | 6/20/08 |
| E2_48042_STD_F177 | 6/28/04 | | E2_73550_STD_F177 | 5/15/09 |
| E2_48265_STD_F273 | 7/13/04 | | E2_73587_STD_F273 | 5/17/09 |
| E2_48271_STD_F177 | 7/14/04 | | E2_73593_STD_F177 | 5/18/09 |
| E2_52545_STD_F273 | 5/8/05 | | E2_73816_STD_F273 | 6/2/09 |
| E2_52551_STD_F177 | 5/9/05 | | E2_73859_STD_F273 | 6/5/09 |
| R1_49672_ST6_F176 | 5/11/05 | | E2_74088_STD_F273 | 6/21/09 |
| R1_49729_FN1_F176 | 5/15/05 | | E2_78826_STD_F273 | 5/18/10 |
| E2_52817_STD_F273 | 5/27/05 | | E2_78869_STD_F273 | 5/21/10 |
| E2_53052_STD_F177 | 6/13/05 | | E2_79061_STD_F177 | 6/4/10 |
| E2_53275_STD_F273 | 6/28/05 | | E2_79098_STD_F273 | 6/6/10 |
| R1_50515_ST3_F176 | 7/9/05 | | E2_79104_STD_F177 | 6/7/10 |
| E2_53547_STD_F273 | 7/17/05 | | E2_79327_STD_F273 | 6/22/10 |
| E2_57784_STD_F273 | 5/9/06 | | E2_79370_STD_F273 | 6/25/10 |
| E2_58013_STD_F273 | 5/25/06 | | | |

Table 3.2: List of the 19 SAR granules used for the analysis of the Upper Kuparuk River. Granule name and date of satellite acquisition are listed. The prefix E2 refers to the ERS-2 satellite and R1 means the granule is from the RADARSAT-1 satellite.

| Granule | Date | | Granule | Date |
|---|---|---|---|---|
| R1_49308_FN1_F278 | 4/15/2005 | | R1_55182_ST3_F278 | 5/31/2006 |
| R1_49872_FN1_F172 | 5/25/2005 | | E2_58105_STD_F173 | 6/1/2006 |
| E2_57784_STD_F277 | 5/9/2006 | | R1_55282_ST3_F278 | 6/7/2006 |
| E2_57833_STD_F173 | 5/13/2006 | | R1_55317_ST3_F173 | 6/10/2006 |
| R1_54939_ST3_F278 | 5/14/2006 | | E2_58285_STD_F277 | 6/13/2006 |
| E2_57876_STD_F173 | 5/16/2006 | | R1_55417_ST2_F172 | 6/17/2006 |
| R1_54982_ST2_F278 | 5/17/2006 | | E2_58377_STD_F173 | 6/20/2006 |
| R1_54996_ST6_F278 | 5/18/2006 | | R1_55503_ST6_F172 | 6/23/2006 |
| R1_55039_ST4_F278 | 5/21/2006 | | R1_55539_ST7_F278 | 6/25/2006 |
| R1_55074_ST2_F172 | 5/24/2006 | | | |

To facilitate the main objectives of this study, the analysis of river breakout timing, SAR data was extracted from the archive for a date range that spanned early May through July for the Lower Kuparuk River, and late April through June for the Upper Kuparuk River. 65 granules covering the Lower Kuparuk River study area were downloaded for the ten-year time span of this investigation and 19 granules from the Upper Kuparuk River study area were acquired for a smaller two-year analysis. The list of SAR granules and their acquisition dates are recorded in Tables 3.1 and 3.2.

Additionally, approximately 25 Landsat images of the Kuparuk River watershed with a 30-meter spatial resolution were obtained. These images served as a proxy for years where SAR and Landsat temporal frequencies overlapped, as well as a visual reference during preprocessing to address concern that the channels of the Lower Kuparuk River, in particular, were possibly shifting course over time. Due to the high occurrence of clouds obscuring the study area, many available Landsat images could not be used. However, by comparing a September 6, 1986

Landsat 5 image to several Landsat images acquired during the 2000s, it was determined that there has been no significant shift in the channels of the Lower Kuparuk River in recent years. Since no shift was noted in the location of the channels it is possible that the Lower Kuparuk River may be an anastomosed system rather than braided. It is also likely that some minimal shifts in channel morphology had occurred but were too small to be noticed at a 25-meter spatial resolution.

A Landsat 7 image from August 25, 2002 was used to trace the river centerlines of all river channels for later masking, which is shown in Figure 3.5. Tracing the river centerline from topographic maps of the area was also a consideration, but was rejected because the maps had not been updated in several decades and did not always accurately reflect the path of the river. Topographic map quadrants that were inspected for this purpose include Beechey Pt., Sagavanirktok, and Phillip Smith Mountains.

Preprocessing of the remote sensing data also required the use of a digital elevation model (DEM). A DEM of the entire North Slope was dowloaded from the Toolik Field Station's GIS archives (Toolik Field Station, 2012).

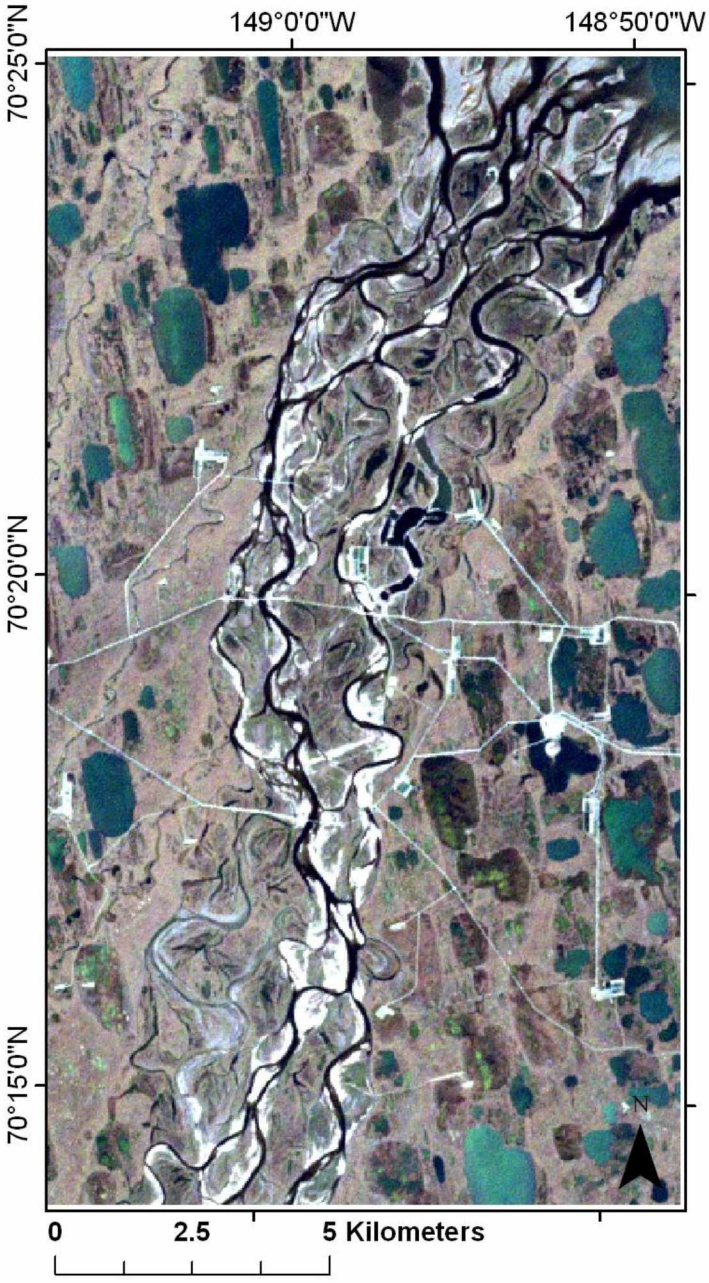


Figure 3.5: Subset of an August 25, 2002 Landsat 7 image of the Lower Kuparuk River. Band combination 3-2-1 is displayed. This image was used to digitize a line file of the river channels. Open water is clearly visible as a dark signature in the channels.

### 3.2.2 GIS Layers

GIS layers used in the creation of study area maps were downloaded from the Alaska State Geospatial Data Clearinghouse (AGDC, 2012). Shapefiles of the State of Alaska, the Colville River, Kuparuk River, Sagavanirktok River, Dalton Highway, and lakes were obtained. Topographic map quadrants at the 1:250,000 scale include Beechey Pt., Sagavanirktok, and Phillip Smith Mountains. Point locations for the two gauging stations were created in ArcGIS based on coordinate measurements from the WERC (Kane and Hinzman, 2012) and USGS (USGS, 2012) websites.

### 3.2.3 Ancillary Data

Meteorological information for the Lower Kuparuk River region has been recorded by the climate station located at the airport in the nearby town of Deadhorse, Alaska (station identifier PASC). Hourly measurements of temperature, wind speed, wind gusts, and precipitation from May 2000 through July 2010 were provided by Edward Plumb at the National Weather Service. Meteorological data for the Upper Kuparuk River site was provided by the UAF WERC Upper Kuparuk climate site (Kane and Hinzman, 2012). Discharge data for the Upper Kuparuk River was also acquired from the WERC online archives in the form of a table of hourly measurements. Discharge information for the Lower Kuparuk River has been published by the USGS as daily measurements (USGS, 2012). Flow measurements from the Upper Kuparuk River were averaged into a daily mean to match the measurement frequency of the USGS gauging station further downstream.

A time-lapse camera was installed near the USGS gauging station on the Lower Kuparuk River for one week from June 1, 2012 – June 8, 2012. Having a series of still images of the river surface during breakup would aid in understanding some of the confounding signals presented in the SAR imagery. Unfortunately, logistics prevented the camera from being set up prior to breakup and most of the ice had already been washed out.

### 3.3 Lower Kuparuk River Workflow

The workflow followed in this study can be divided into three main sections: preprocessing, wind correction, and statistical backscatter analysis. Preprocessing steps were standard image processing procedures, though an additional step of Fast Fourier Transform (FFT) matching was introduced to improve significant geocoding inaccuracies. The wind correction and analysis sections were both modeled after examples taken from literature, most notably the publication by Unterschultz *et al.* (2009).

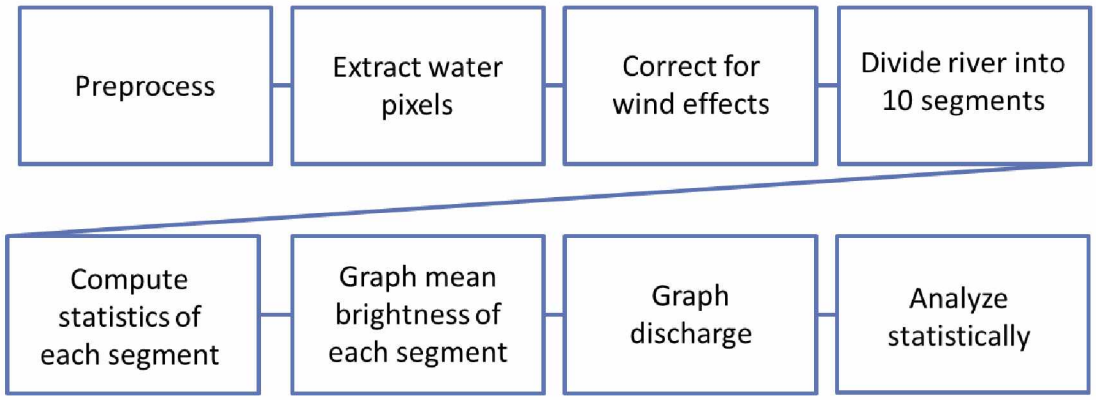


Figure 3.6: The processing strategy for the Lower Kuparuk River dataset. Diagram reads from left to right.

Processing began with data from the Lower Kuparuk River and is outlined in Figure 3.6. After downloading data from the Alaska Satellite Facility (ASF) archives, the first step was preprocessing, which required the images to be geocoded to the WGS84 UTM Zone 6N map projection, assigning the pixel size to 12.5 meters, and rescaling the image into sigma dB. The ASF software package MapReady was used for this processing (Gens and Logan, 2003). A shapefile of the Lower Kuparuk River study area was created in ESRI ArcMap 9.3. Geocoded images, output from MapReady, were stacked and loaded into the image processing software Envi© to be subset to the study area using the previously created polygon shapefile of the Lower Kuparuk River study area. Images were clipped to this area and saved as GeoTIFFs.

As discussed in section 3.2, the river channels of the Lower Kuparuk River were traced using a Landsat image. The river centerline was created as a polyline in ArcMap and used extensively for reference purposes. Subsets spanning the temporal series of the Lower Kuparuk River were visually compared in ArcMap to see if any obvious changes occurred in the backscatter of the river from May to July that might aid in distinguishing the breakup event. Many of the geocoded subsets did not properly overlay. Imprecise orbits of both satellites, and therefore imprecise telemetry data, was the root cause of the geocoding mismatch and was remedied through a fast fourier transform as part of preprocessing.

The second step in processing workflow was extracting the river pixels so they could be analyzed without considering the statistics of the surrounding terrain. A 25-meter buffer was applied to the river centerline and then rasterized. This rasterized buffer was then converted to a mask which would extract just the river pixels within the buffer. A mask functions using basic

principles of image multiplication. All desired pixels in the mask file are assigned a value of one and all unwanted pixels assigned to zero. When the mask file is multiplied by the subset, all the pixels multiplied by zero in the mask are removed from the output image and only the pixels multiplied by one are extracted.

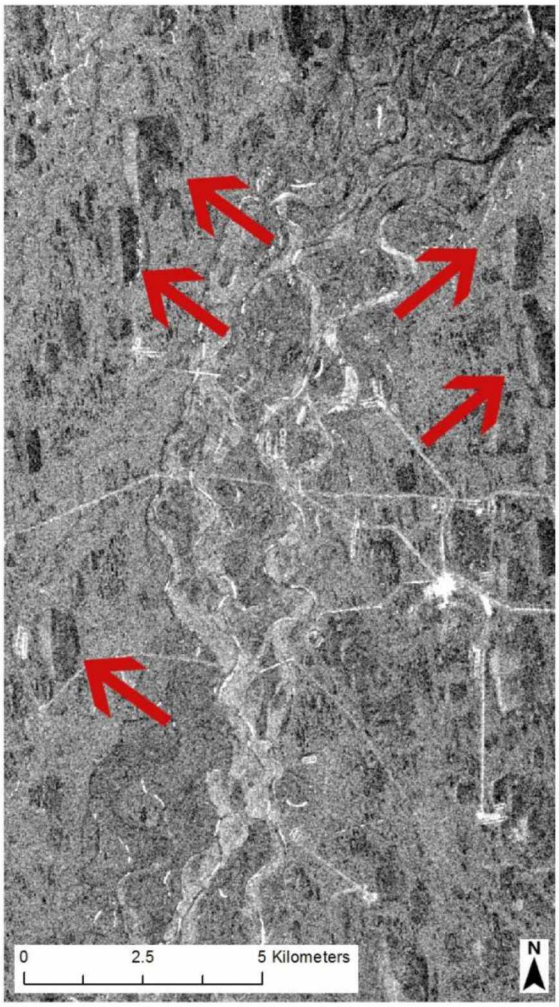


Figure 3.7: SAR subset from May 14, 2007 showing a frozen Lower Kuparuk River. Red arrows point to lakes that have snow drifts on the western side. Wind direction on this day was at 230°.

Prior to masking the images it was apparent from the visual inspection of Lower Kuparuk River subsets that many of the images had an unclear spatially variable backscatter response, at times making it difficult to distinguish the river from the background landscape. Such variable signatures could be caused by wind. Wind is a prominent characteristic of this environment, and its influence can be best seen if attention is focused on the large lakes surrounding the river (Figure 3.7). One can easily see that the snow cover on the frozen lakes has been blown to one side and is uniform on all the lakes. The redistribution of snow and ice as a result of changing wind patterns leads to complications in backscatter interpretation. Wind likely played a role in causing unclear signals noted in a variety of post-breakup images. These subsets sometimes looked similar to pre-breakup images taken in early to mid-

May, with the river appearing quite bright in comparison to the surrounding topography. Figure 3.8 is a comparison between a pre-breakup (Figure 3.8A) image and a post-breakup image from a windy day (Figure 3.8B). Both images show a high backscatter response over the river that makes it difficult to use raw backscatter response as a basis for either visual or statistical interpretation. Post-breakup, wind can cause small waves on the water surface which could potentially increase the average backscatter at wind driven river segments, as seen in Figure 3.8B. An objective of this study is to report on any variances occurring around the breakup time and the wind effect could be masking other signals and influencing this variance. Therefore, after extracting the water pixels a correction for wind effects was implemented.

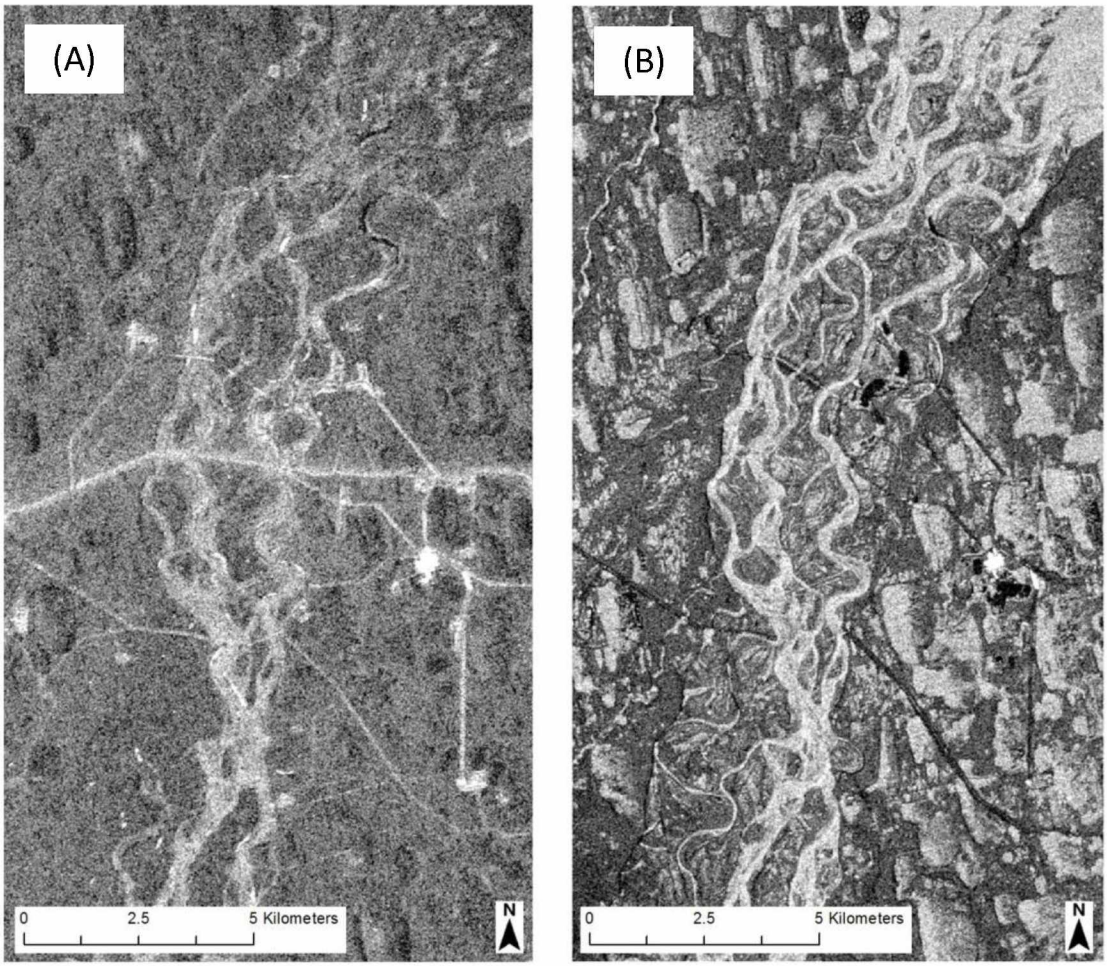


Figure 3.8: SAR images from a windy and a non-windy day. Comparison of a subset from May 14, 2008 (A) showing a frozen Lower Kuparuk River, and a June 4, 2010 (B) subset with significant backscatter caused by high winds (wind gusts on this date reached 48 mph). The June 4 subset is near the peak of the breakup flood and water is moving through the channel. However, the river appears very bright and shares many of the visual characteristics of the frozen image.

An attempt to correct for wind effects was carried out by graphing wind speed against the mean brightness of the entire extracted river length, and fitting a regression line through the points, a methodology which was adapted from Horstmann *et al.* (2003). Wind speeds were retrieved from the meteorological archives provided by NOAA and the measurement taken most closely

to the time of image acquisition was used. The National Oceanic and Atmospheric Administration's (NOAA) Deadhorse climate station records hourly conditions, so the timing difference between SAR image acquisition and a meteorological report was small, typically on the order of about twenty minutes.

A separate analysis of wind influence was carried out for each hydrological period: pre-breakup, breakup, and post-breakup. Images were assigned to each plot based on the relation of the acquisition date to the flood event as defined by the stream gauge measurements. A goodness of fit analysis was carried out for every regression model by calculating the coefficient of determination – $R^2$ – taking the square root, and comparing the results to the Pearson Product-Moment Correlation Coefficient table of critical R values. Image brightness values from all river segments of the Lower Kuparuk were fitted to the regression line of the hydrological period in which they fell. Results of the wind correction procedure as well as results from the wind correction analysis are included in Section 4.1.

The fourth processing step involved segmenting the Lower Kuparuk River study area shapefile into ten equal sections (Floyd *et al*., 2011). Segmenting the river allowed local changes in the river surface to be captured, while still allowing for enough pixels to perform a statistical analysis. Each section was slightly over two kilometers in length, based on latitude. The original study area polygon was copied then divided into ten equal rectangles using the Create Fishnet Tool in ArcGIS. The segments were numbered one through ten starting at the northernmost rectangle, as illustrated in Figure 3.9. Using the Clip Tool, every masked subset was clipped into

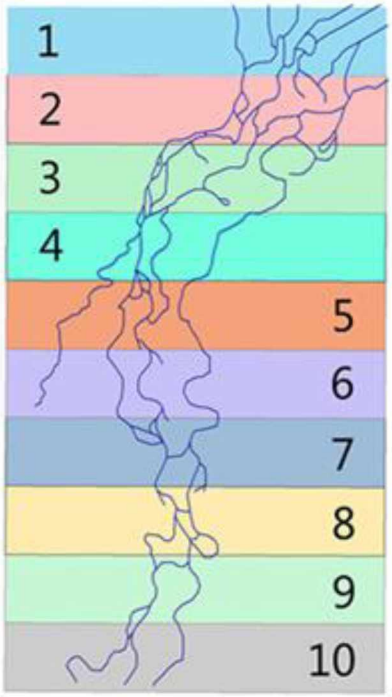


Figure 3.9: The ten river segments the Lower Kuparuk River study area was divided into. Each segment is labeled with a different symbol.

ten segments. The mean dB value of each segment was calculated using the image statistics function and recorded.

The ten segments spanned just over twenty kilometers and the first two segments contain portions of the river delta, which complicates the interpretation of the SAR signal. The mixture of fresh and saline water alters the dielectric constant and introduces confounding signals to the imagery. Due to the deltaic influences, and very near the coast the tidal influences as well, segments one and two of the Lower Kuparuk River study area were removed from the analysis.

After segmenting the river and computing the statistics of each segment, the hydrograph data were plotted. On the same graph, the statistics of each river segment were also plotted, for further analysis of three variables believed to be possible breakup indicators: segment brightness, brightness variance between river segments, and the sum of segment rank order changes. Mean segment brightness in dB was plotted on the y-axis and the date of image acquisition on the x-axis. A data point was derived per river segment and acquisition time, and each of the eight river segments was labeled with its own unique symbol, so that the response of each river segment was evident in the plot of brightness values from dates of SAR acquisitions. River discharge data was plotted on a secondary y-axis and the breakup flood event is illustrated as the first curve on the hydrograph. Rainfall events post-breakup often appear as smaller curves, though in some cases eclipse the peak discharge of the

breakup flood and are larger curves than the breakup event. A notation of “A” or “D” has been made on the graphs by each image date to indicate whether the data was acquired in an ascending or descending mode.

The variance and standard deviation (square root of the variance) denoting the brightness variation between all river segments in each image was calculated and recorded in a table. The image date with the highest variance (or standard deviation) was highlighted. Additionally, the mean brightness of each segment was ranked, with the brightest segment given a ranking of one and the darkest segment assigned a rank of eight. In instances where two segments had exactly the same mean brightness, they were assigned the same rank.

To analyze the pattern of change during the pre-breakup phase and the post-breakup phase, a sum of rank order change analysis was carried out. Sum of rank order change (SROC) analysis first involved calculating the change in rankings of the segments over a temporal image stack. This is done using equation 3.1:

$$[3.1] \qquad |\text{segment}_n\text{image}_1 - \text{segment}_n\text{image}_2| = \Delta\text{rank}_{\text{segment n}}$$

where $\text{image}_1$ is the earlier date image and $\text{image}_2$ is the following date image in the chronological sequence.

If segments maintained the same rank in successive images, the change in rank would be zero and if they moved from the highest ranking of one to the lowest ranking of eight, or vice versa,

the change would be seven (note that direction of change is not important and therefore only an absolute rank number was reported). Equation 3.2 describes this step.

$$[3.2] \qquad (\mathrm{SROC} = \sum_{n=1}^{N} \Delta \mathrm{rank}_{\mathrm{segment}_n}) \tag{3.2}$$

The sum of all rank changes for segments 3-10 between successive image pairs was calculated to give one value representing the magnitude (summative value) of change in rank order.

The rationale for carrying out the sum of rank order change analysis was that during pre-breakup stage there would be minimal changes in the surface characteristics of the frozen river. However, during breakup and post-breakup stages the river surface would have considerable spatial and temporal heterogeneity, due to the mixing of open water, fractured ice, and stable ice. Given this behavior, we expected the sum of rank order changes to be low during pre-breakup and higher during and after breakup. Any significant increase in the summative value of the rank order changes, referred to as the sum of rank order changes, could therefore serve as an indicator of breakup onset.

### 3.4 Upper Kuparuk River Workflow

The Upper Kuparuk River is much narrower than the Lower Kuparuk River with a single channel and gravel bars. In some cases growth of vegetation on the bars has formed small islands. The standard beam SAR pixel size is 12.5 meters (used for the Lower Kuparuk River analysis), which exceeds some parts of the channel width in this area. Since the river is so narrow in this part of the watershed, a statistical analysis is not prudent. Even if only one pixel along the river length

was extracted, it would include a large area of the river banks, bars, islands, and only a fraction of the pixel would depict water. To avoid this mixed pixel effect, a visual analysis was undertaken at this study site.


Figure 3.10: Upper Kuparuk River workflow

The workflow for the Upper Kuparuk River is shown in Figure 3.10 and is comprised of three main steps: preprocessing, a visual analysis, and a comparison of the visual interpretation to actual discharge data. Preprocessing steps for the Upper Kuparuk River are similar to those performed on the Lower Kuparuk River dataset except a terrain correction was also applied due to the topographical variances in this region. SAR scenes were then subset to the study area and analyzed.

The first step in the visual analysis was to scale all the images by manually assigning the same gray value range to all subsets using a Minimum-Maximum stretch and specifying a minimum of -20 dB and a maximum of -5 dB. This ensured a fair comparative analysis of the temporal image stack, without introducing a bias in visual analysis due to unusually high brightness or contrast in an image of a particular date. Discharge data from WERC was plotted and used to help assist SAR data interpretation. Images were viewed consecutively beginning with pre-breakup and

ending with post-breakup. Changes in river appearance were noted for all images. Results from the Upper Kuparuk River visual analysis are presented in section 4.3.

## 4.0 Results

### 4.1 Wind Correction

For all three hydrological periods: pre-breakup, breakup, and post-breakup, a two tailed Pearson Product-Moment Correlation Coefficient test was run to determine if the linear correlation between wind speed and brightness was significant (Floyd *et al*., 2012). Critical R values for this test are published based on the degree of freedom (Siegle, 2012) and compared to the r value from the regression line of each correlation. The $R^2$ value is the coefficient of determination and describes how much of the variance in a particular data set is explained by the regression line. $R^2$ values range from 0 to 1 with larger values indicating a better fit and lower values indicating a poor fit. The r value is the square root of the $R^2$ value and is the correlation coefficient. If the r value (the square root of the $R^2$ value seen on Figures 4.1-4.3) is greater than the critical R listed in the table then the result is significant. If the r value is less than the critical R, then the result is not significant. Significant was tested at $\alpha$= 90%, 95%, 98%, and 99% confidence intervals, but a final determination of significance was assigned based on the 95% confidence level. The results from the more stringent confidence intervals are included to give a more complete picture of the outcome of the test at different levels. The null and alternative hypotheses are the same in each case and are:

$H_0$ = There is no relationship between wind speed and image brightness.

$H_A$ = There is a relationship between wind speed and image brightness

The pre-breakup data shown in Figure 4.1 displays a weak correlation between the wind speed and image brightness, with a regression line that has a slope near zero. 21 samples fall into the pre-breakup period, meaning 19 degrees of freedom were used. The $R^2$ value from Figure 4.1 is 0.2043, and taking the square root of that gives an r value of 0.4520, which can be compared to the critical R at the various confidence intervals. Results from this statistical test are assembled in Table 4.1.

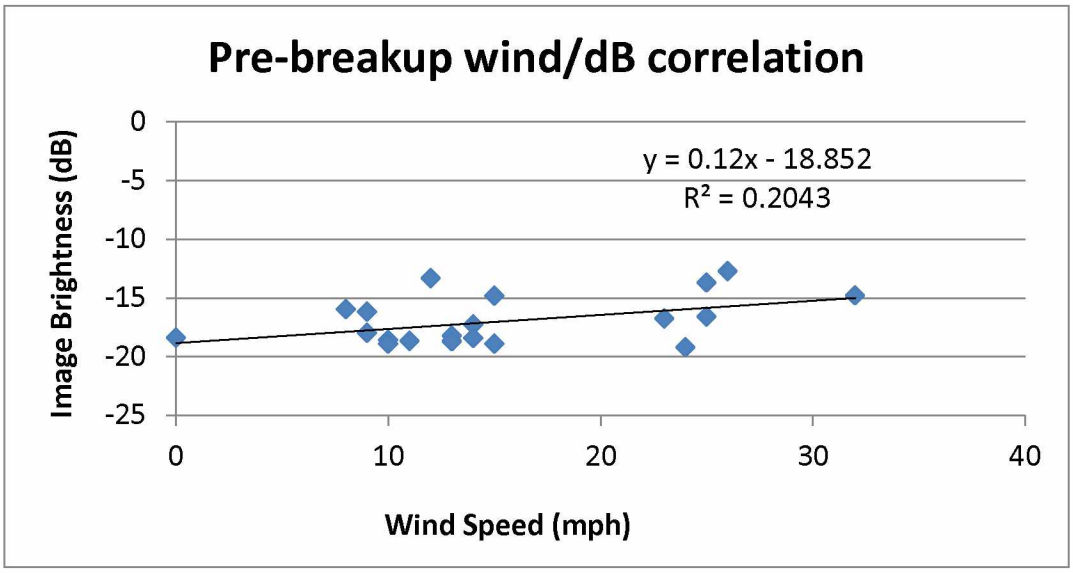


Figure 4.1: Pre-breakup correlation between wind speed and image brightness. For images obtained prior to the breakup flood a weak relationship can be drawn between the two variables.

Table 4.1: Pre-breakup wind correction statistics for the Lower Kuparuk River.

| Confidence Level | Critical R | Significant/Not significant |
|---|---|---|
| 90% | 0.369 | Significant: Reject null |
| 95% | 0.433 | Significant: Reject null |
| 98% | 0.503 | Not significant: Fail to reject null |
| 99% | 0.549 | Not significant: Fail to reject null |

At the 95% confidence interval, the r value of 0.4520 calculated from the $R^2$ value seen on Figure 4.1 is greater than the critical R. Therefore, the correlation is significant and the null hypothesis is rejected in favor of the alternative hypothesis.

During breakup (breakup-time data is shown in Figure 4.2) there appears to be a slightly stronger correlation and the samples are more tightly grouped than in the pre-breakup graph. The plot contains nineteen samples and has seventeen degrees of freedom. The $R^2$ value of this regression line is 0.268, the square root of which is 0.518 (the r value). Results from the test are shown in Table 4.2.

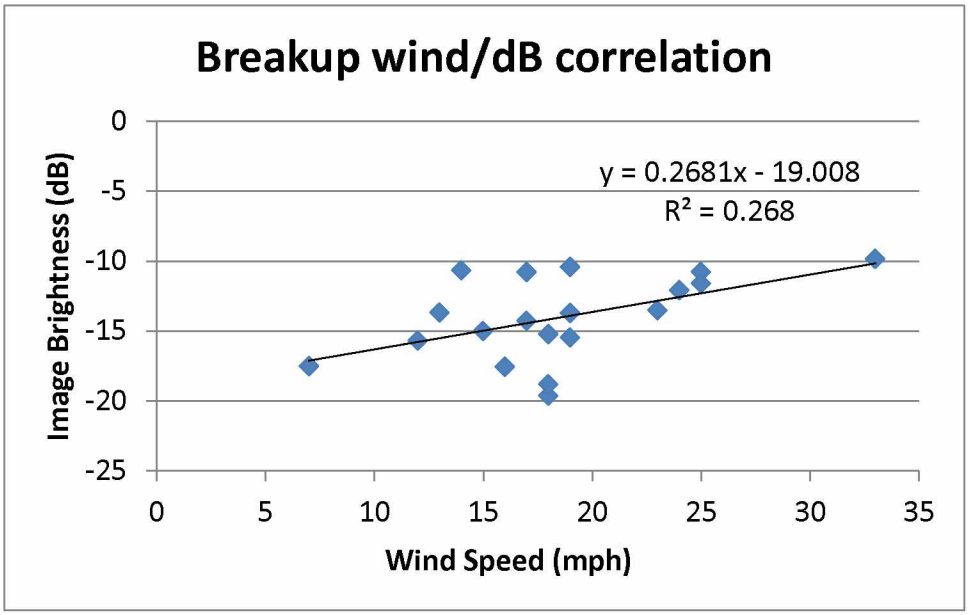


Figure 4.2: Breakup correlation between wind speed and image brightness. Here again a weak correlation can be drawn between wind speed and brightness.

Table 4.2: Breakup wind correction statistics for the Lower Kuparuk River.

| Confidence Level | Critical R | Significant/Not significant |
|---|---|---|
| 90% | 0.389 | Significant: Reject null |
| 95% | 0.456 | Significant: Reject null |
| 98% | 0.528 | Not significant: Fail to reject null |
| 99% | 0.575 | Not significant: Fail to reject null |

Just as in the pre-breakup example, the critical R listed in the table is less than the r value calculated from the regression line on Figure 4.2. Thus, the breakup correlation is significant at the 95% confidence interval and the null hypothesis is rejected.

Post-breakup there is largely no correlation between wind speed and image brightness; both the slope of the trend line and the $R^2$ value in Figure 4.3 are exceedingly low. 25 samples make up the post-breakup plot and there are 23 degrees of freedom in the test. The r value (derived from the $R^2$ value on Figure 4.3) is 0.1456 and results are presented in Table 4.3.

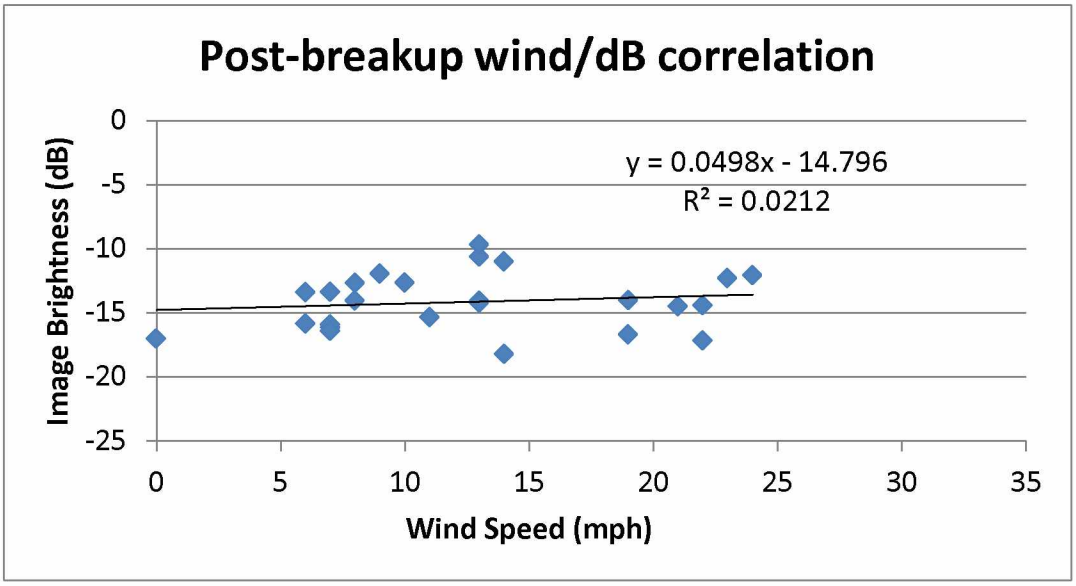


Figure 4.3: Post-breakup correlation between wind speed and image brightness. There is virtually no relationship between the variables at this stage.

Table 4.3: Post-breakup wind correction statistics for the Lower Kuparuk River.

| Confidence Level | Critical R | Significant/Not significant |
|---|---|---|
| 90% | 0.337 | Not significant: Fail to reject null |
| 95% | 0.396 | Not significant: Fail to reject null |
| 98% | 0.462 | Not significant: Fail to reject null |
| 99% | 0.505 | Not significant: Fail to reject null |

The critical R value is greater than the r value calculated from the regression line in Figure 4.3. Not surprisingly, the test fails to reject the null at all confidence intervals and it is inferred that there is no correlation between wind speed and image brightness in the post-breakup images.

As the data at two of the three time frames show significant correlation with wind speed, and to apply a consistent data processing flow to all images in the pool, it was decided to apply wind speed correction to all data sets analyzed in this study including the post-breakup acquisitions.

**4.2 Lower Kuparuk River**

Tables 4.4 -4.23 and Figures 4.4-4.13 show input data information and breakup sequence graphs from the Lower Kuparuk River for each year. The Lower Kuparuk River analysis for each year are presented and discussed in this section. For each year the results include (a) table showing essential image and field information, (b) a graph showing the breakup sequence, and (c) another table highlighting the sum of rank order change analysis.

All tables show essential image characteristics and pertinent field data. Annotations A and D indicate whether the image was acquired in an ascending or descending mode. The polarization mode of the SAR image (ex: whether it was a horizontal signal with horizontal return (HH) or a vertical signal with a vertical return (VV) is also indicated. Image brightness was not a useful criterion and hence not reported on the tables. The variance is reported on the tables and the highest variance in each year is highlighted. The image acquisition time along with the closest field data record is noted.

All graphs are scaled identically on both the primary and secondary y-axis and have a temporal frequency of ten days on the x-axis. The primary y-axis displays the mean dB value of each segment from every image date, taken from the river channel mask. Discharge data from the USGS gauging station at the Lower Kuparuk River is shown in blue on the secondary y-axis.

### 4.2.1 Year 2001

Results and analysis from the Lower Kuparuk River for the year 2001 are shown in Tables 4.4-4.5, and Figure 4.4.

Table 4.4: 2001 Lower Kuparuk River image information, statistics and weather data. Date with highest variance is highlighted.

| Image Date | Variance | Stdv | Time of SAR Acquisition | Time of Weather Report | Temp (°C) | A/D | HH/VV |
|---|---|---|---|---|---|---|---|
| May 29 | 0.739 | 0.860 | 16:58 | 16:53 | -10.6 | D | HH |
| May 31 | 0.431 | 0.656 | 21:24 | 21:53 | 0.56 | D | VV |
| June 12 | 0.782 | 0.884 | 03:13 | 2:53 | 5.56 | A | HH |
| June 22 | 0.232 | 0.482 | 21:33 | 21:53 | 3.89 | D | VV |

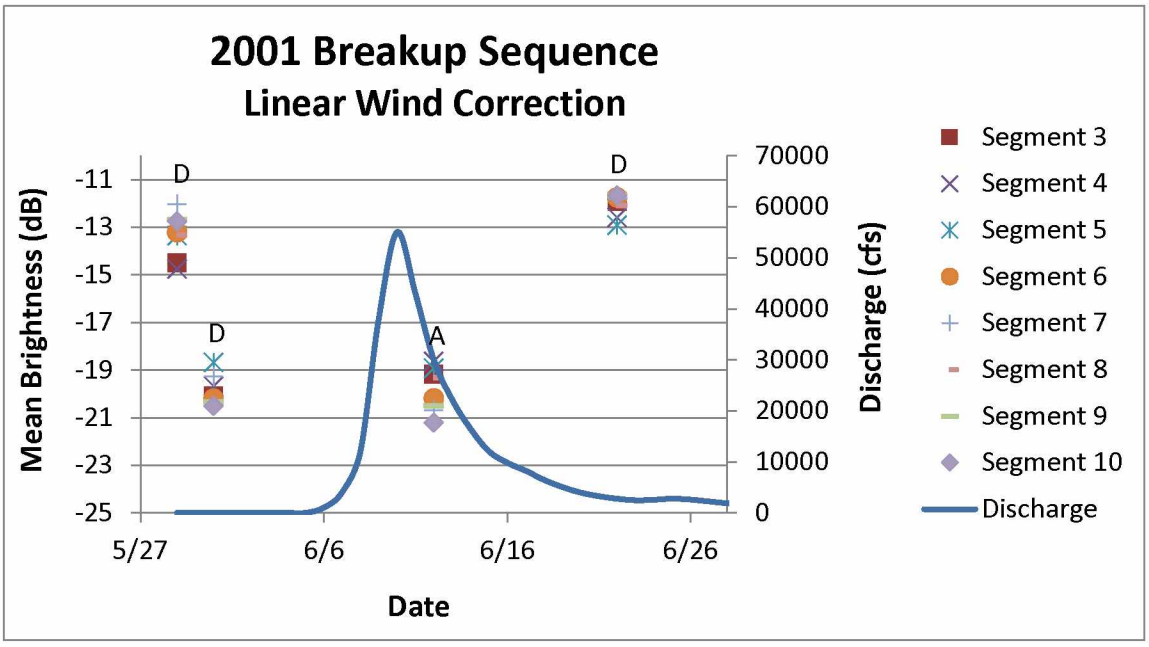


Figure 4.4: 2001 Lower Kuparuk River breakup sequence. The plot displays similar patterns during pre-breakup and an opposite pattern during the breakup event. A relatively bright response with low variance is observed post-breakup.

Table 4.5: Sum of rank order changes between river segments for 2001

| **Image Pair** | May 29/May 31 | May 31/June 12 | June 12/June 22 |
|---|---|---|---|
| **Sum of Rank Order Δ** | 27 | 13 | 31 |

In Figure 4.4 it can be seen that prior to breakup, the two descending satellite passes on May 29 and May 31 both have large variances in brightness throughout the river length. The ten segments plot between -12 and -14.5 dB for May 29 and between -18.7 and -20.5 for May 31. The image from May 31 is less bright than the previous image likely as a result of microwave interaction with the surface of the ice. The ascending pass, from which the June 12 image was generated, also has the largest spread of brightness values from the different river segments and has a variance of 0.782, as seen in Table 4.4. Discharge was first measured on June 6 at a rate of 1,000 cfs. On June 12, the mean discharge was recorded at 30,000 cfs and this is the only breakup image in the time series. The highest rate of discharge reported occurred two days before, on June 10 at 55,000 cfs. Since the June 12 image was acquired after the height of the flood, there was likely mostly open water at this time. Ice may have been stranded in some smaller channels or on the banks causing the variance in brightness found in this image.

An image from June 22 serves as a representation of the post-breakup period. On this date mean discharge was recorded as 2,760 cfs and the water level must have dropped considerably. This image is bright, with all segments registering a mean dB value between -11.6 and -13. Segments 3, 6, 7, 8, 9, and 10 are tightly grouped around -11.6 dB and segments 4 and 5 appear slightly less bright but are also closely spaced at -12.61 and -12.82 dB. The bright response from

this time may be due to scattering caused by more sediment from the river banks being exposed since the water level had dropped.

The sum of rank order changes of the river segments in the SAR series, seen in Table 4.5, shows a large fluctuation in the pattern of segment response between the May 29 and May 31 images with a rank change sum value of 27. For the next image pair, May 31 and June 12, this value is only 13, which is nearly half of the value for the preceding image pair – an observation that is difficult to explain without concurrent field information. Looking at the graph in Figure 4.4, a similarity in the order in which the segments plot can be seen implying that the river segments responded in a similar way in both images. This similarity is counter-intuitive. The last image pair between June 12 and June 22 has a high ranking of 31, indicating image segments have shifted order and river segments have varying levels of backscatter between the two images. Therefore, the proposed sum of rank order change method to bracket breakup did not work in the case of the 2001 images.

### 4.2.2 Year 2002

Results and analysis from the Lower Kuparuk River for the year 2002 are shown in Tables 4.6-4.7, and Figure 4.5.

Table 4.6: 2002 Lower Kuparuk River image information, statistics, and weather data. Date with highest variance is highlighted.

| Image Date | Variance | Stdv | Time of SAR Acquisition | Time of Weather Report | Temp (°C) | A/D | HH/VV |
|---|---|---|---|---|---|---|---|
| May 3 | 0.214 | 0.462 | 21:32 | 21:53 | -11.11 | D | VV |
| June 8 | 0.022 | 0.148 | 07:25 | 7:53 | 5 | A | VV |
| June 23 | 0.110 | 0.331 | 21:29 | 21:53 | 2.22 | D | VV |
| July 9 | 0.718 | 0.847 | 21:26 | 21:53 | 12.78 | D | VV |

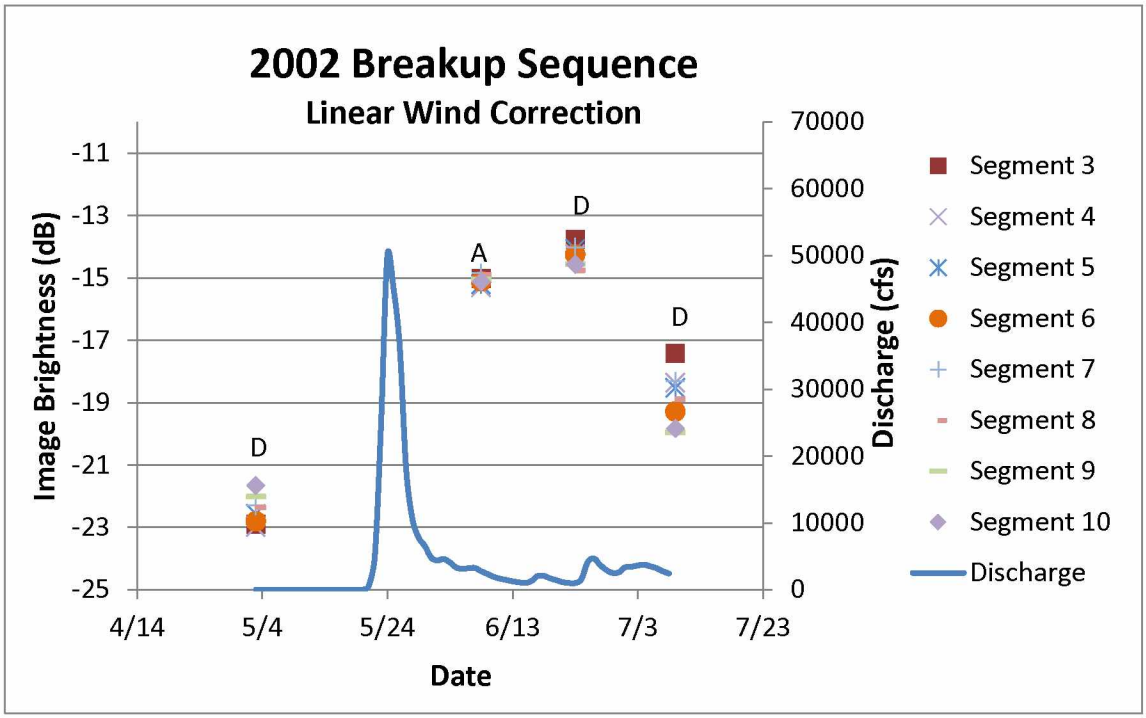


Figure 4.5: 2002 Lower Kuparuk River breakup sequence. The hydrograph from this year displays a swift and sudden flood event.

Table 4.7: Sum of rank order changes between river segments for 2002

| **Image Pair** | May 3/June 8 | June 8/June 23 | June 23/July 9 |
|---|---|---|---|
| **Sum of Rank Order Δ** | 16 | 22 | 8 |

Data from 2002 is sparse and no imagery was available during the breakup event, as evident in Figure 4.5. The runoff measurements do not coincide with any SAR acquisitions, so this year does not make a useful addition to the analysis. A rainfall event is evident in late June, peaking on June 25 and causing a small rise in discharge. The next SAR image is from July 9 and has the greatest variance of the four images from that year (see Table 4.6). In other years, the variance is greatest around the breakup initiation, but due to the scarcity of data in 2002, the late summer image turns out to be the most variable. It can be proposed that because of the very steep and sudden increase in discharge, which began on May 31 with 10 cfs and peaked on June 7 at 43,000 cfs, 2002 leaned strongly towards a mechanical breakup.

The results of the sum of rank order change analysis compiled in Table 4.7 suggest a moderate change in the order that segments plotted during breakup, with the sum of rank order changes equaling sixteen. The sum of rank order change increased to 22 between the two post-breakup images June 8 and June 23, but then fell dramatically to eight for the last set of post-breakup images from June 23 and July 9. Between the last image pair acquisitions, the river surface quite likely remained homogenous due to smooth calm flows. This caused many visual and statistical similarities as river segments responded with similar backscatter amounts in both images, resulting in the lack of shifts in rank order. The paucity of pre-breakup images makes it difficult to use this image series to bracket the breakup time.

### 4.2.3 Year 2003

Results and analysis from the Lower Kuparuk River for the year 2003 are shown in Tables 4.8-4.9, and Figure 4.6.

Table 4.8: 2003 Lower Kuparuk River image information, statistics, and weather data. Date with highest variance is highlighted.

| Image Date | Variance | Stdv | Time of SAR Acquisition | Time of Weather Report | Temp (°C) | A/D | HH/VV |
|---|---|---|---|---|---|---|---|
| May 4 | 0.748 | 0.865 | 21:29 | 21:00 | -8.89 | D | VV |
| May 5 | 0.797 | 0.893 | 07:22 | 06:53 | -8.89 | A | VV |
| June 6 | 0.285 | 0.534 | 07:16 | 06:53 | 1.67 | A | VV |
| June 8 | 1.582 | 1.258 | 21:29 | 21:53 | 3.33 | D | VV |
| June 27 | 0.081 | 0.285 | 21:32 | 21:53 | 7.78 | D | VV |

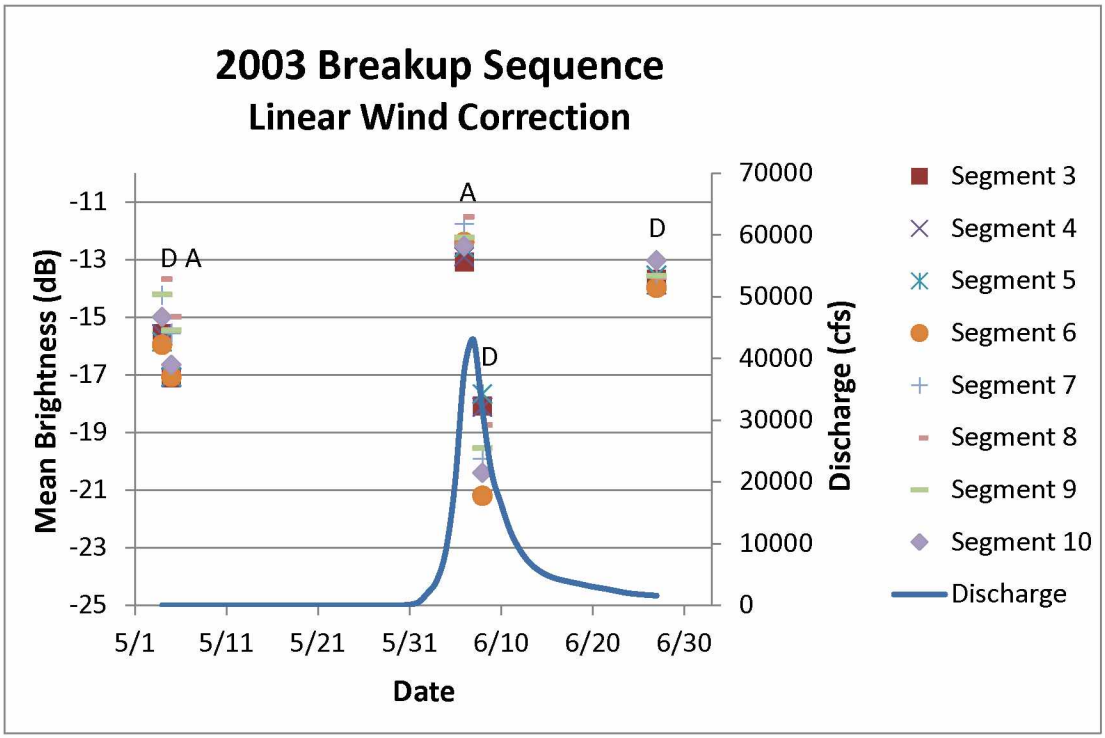


Figure 4.6: 2003 Lower Kuparuk River breakup sequence. There is a noticeably high variance between river segments during the breakup flood and a low variance bright response post-breakup.

Table 4.9: Sum of rank order changes between river segments for 2003

| **Image Pair** | May 4/May 5 | May 5/June 6 | June 6/June 8 | June 8/June 27 |
|---|---|---|---|---|
| **Sum of Rank Order Δ** | 7 | 7 | 30 | 22 |

The 2003 breakup sequence is an excellent example of the large variance at breakup as originally anticipated. Table 4.8 contains the variances from this year. The runoff data in Figure 4.6 is succinct with a clear and simple curve showing the peak discharge on June 7 with 43,000 cfs. SAR images from June 6 and June 8 – a day before and after the peak flow – are available for this year. The mean brightness values of all the segments from the June 6 image are in a

relatively tight cluster with dB values ranging from -12.54 to -11.41. As a whole, the segments from this date appear brighter than the other images in the sequence. This may be a result of meltwater breaking and shifting the ice. The freshly broken surfaces of the ice, combined with the surface water may have scattered incoming microwaves leading to the bright signature reported. The high variance in the June 8 image, which is the largest variance in the 2003 series, is likely caused by the combination of open water and ice in the river. Post-breakup there is a bright, low variance image from June 27. This type of signature is common after the breakup has passed and may be due to scattering from turbulent or sediment-rich water.

The sum of rank order change analysis for this year, in Table 4.9, is promising. It shows that although the overall brightness between the May 4 and May 5 scenes shifted up and down, the relative brightness of each segment remained fairly stable. The sum of rank order change between these two dates is only seven. More promising still is the fact that the change in rank order between the May 5 and June 6 image, acquired very close to the peak discharge, is also seven. However, the rank orders are greatly shuffled between the June 6 and June 8 acquisitions, with the sum of rank order change rising to 30. The sum of rank order changes remain high for the next image pair between June 8 and June 27, with a sum of rank order change of 22. During the last two image pairs there were likely a lot of changes occurring on the river surface causing segments to become either brighter or darker in successive images and raising the sum of rank order change value considerably in the late image pairs compared to the earlier image pairs.

### 4.2.4 Year 2004

Results and analysis from the Lower Kuparuk River for the year 2004 are shown in Tables 4.10-4.11, and Figure 4.7.

Table 4.10: 2004 Lower Kuparuk River image information, statistics, and weather data. Date with highest variance is highlighted.

| Image Date | Variance | Stdv | Time of SAR Acquisition | Time of Weather Report | Temp (°C) | A/D | HH/VV |
|---|---|---|---|---|---|---|---|
| May 7 | 0.035 | 0.188 | 21:32 | 21:53 | -12.22 | D | VV |
| May 21 | 0.146 | 0.382 | 07:16 | 06:53 | 0 | A | VV |
| June 8 | 0.391 | 0.625 | 21:26 | 21:53 | 2.78 | D | VV |
| June 25 | 0.193 | 0.439 | 7:16 | 6:53 | 5.56 | A | VV |
| June 27 | 0.125 | 0.354 | 21:29 | 21:53 | 16.11 | D | VV |

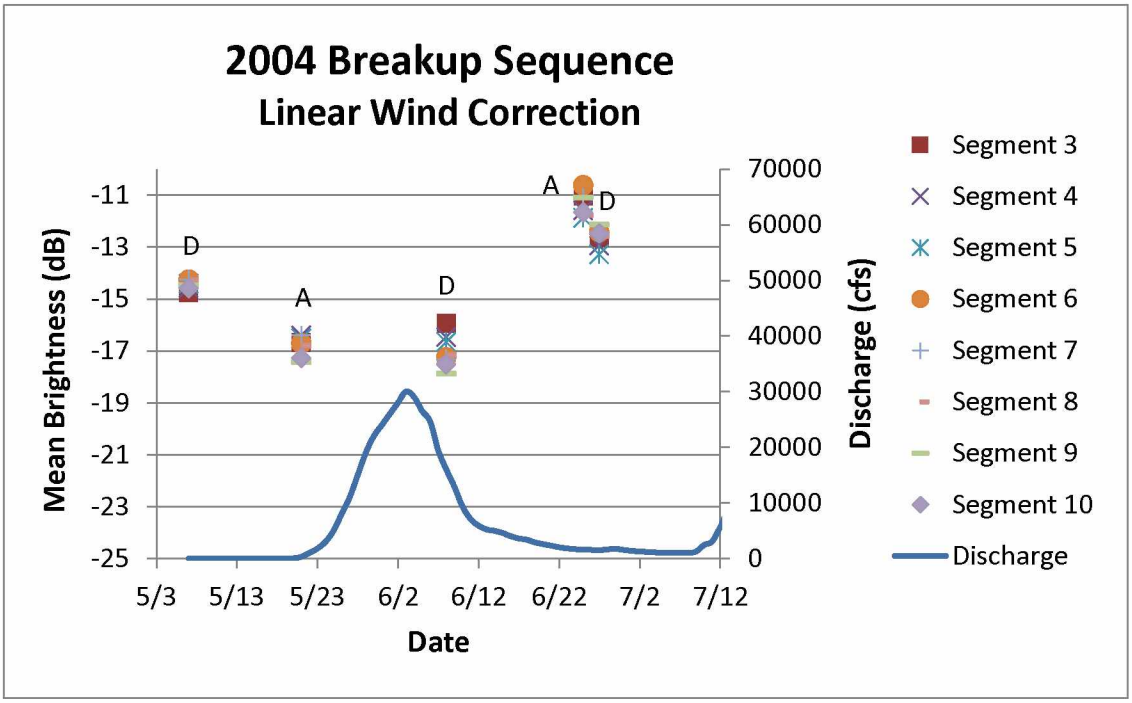


Figure 4.7: 2004 Lower Kuparuk River breakup sequence. There was a higher variance during breakup, but generally lower variances than in other years.

Table 4.11: Sum of rank order changes between river segments for 2004

| **Image pair** | May 7/May 21 | May 21/June 8 | June 8/June 25 | June 25/June 27 |
|---|---|---|---|---|
| **Sum of Rank Order Δ** | 19 | 10 | 24 | 12 |

The 2004 plot (Figure 4.7) is characterized by a general lack of variance in the majority of the images, the data for which is compiled in Table 4.10. Peak discharge was reported on June 3 with 30,000 cfs and the SAR image closest to this date was taken on June 8 and has the highest variance. Again a bright, low-variance signal is reported post-breakup. In fact both post-breakup images from 2004 - June 25 and June 27 - follow this pattern.

The sum of rank order change analysis in Table 4.11 shows a moderate change in relative segment brightness over the entire time series, though between May 21 and June 8 there seem to be minimal shifts. As these images fall on either side of breakup time, this is a confusing signal that does not make sense. Between the June 8 and June 25 acquisitions the sum of rank order change increased to 24. During this time discharge dropped and a smaller volume of water was filling the channels, which may have led to a change in brightness response amongst some of the river segments, in comparison to others. The final post-breakup image pair from June 25 and June 27 has a smaller sum of rank order change of 12, which could be because river conditions were fairly stable with no precipitation events and minimal discharge.

### 4.2.5 Year 2005

Results and analysis from the Lower Kuparuk River for the year 2005 are shown in Tables 4.12-4.13, and Figure 4.8.

Table 4.12: 2005 Lower Kuparuk River image information, statistics, and weather data. Date with highest variance is highlighted.

| Image Date | Variance | Stdv | Time of SAR Acquisition | Time of Weather Report | Temp (°C) | A/D | HH/VV |
|---|---|---|---|---|---|---|---|
| May 8 | 0.507 | 0.712 | 21:29 | 21:53 | -7.22 | D | VV |
| May 9 | 0.471 | 0.686 | 02:50 | 02:53 | -6.67 | A | VV |
| May 11 | 0.402 | 0.634 | 03:32 | 03:53 | -6.67 | A | HH |
| May 15 | 0.350 | 0.592 | 03:15 | 02:53 | -4.44 | A | HH |
| May 27 | 1.743 | 1.320 | 21:32 | 21:53 | 0 | D | VV |
| June 13 | 0.571 | 0.756 | 07:22 | 06:53 | 0 | A | VV |
| June 28 | 0.352 | 0.594 | 21:26 | 21:53 | 16.11 | D | VV |

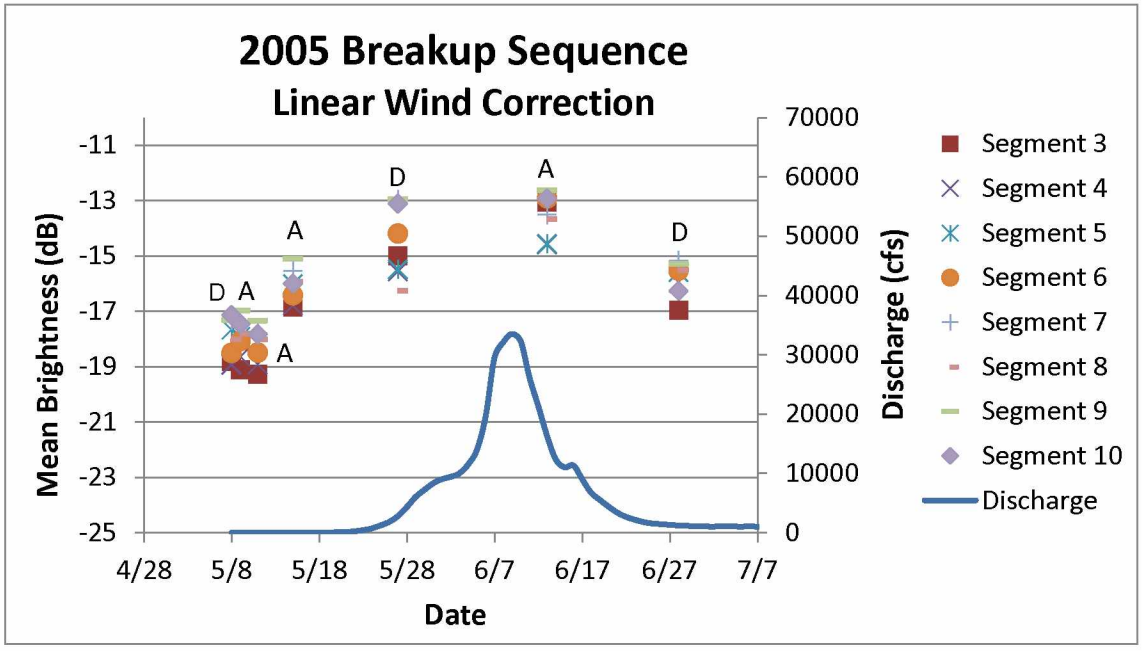


Figure 4.8: 2005 Lower Kuparuk River breakup sequence. A high variance can be seen on all image dates.

Table 4.13: Sum of rank order changes between river segments for 2005

| **Image Pair** | May 8/May 9 | May 9/May 11 | May 11/May 15 | May 15/May 27 | May 27/June 13 | June 13/June 28 |
|---|---|---|---|---|---|---|
| **Sum of Rank Order Δ** | 8 | 0 | 2 | 12 | 10 | 20 |

In contrast to the preceding year, 2005 is marked by a high variance in all the SAR images. Variances from all image dates can be seen in Table 4.12. 2005 also has a long period of low discharge which slowly increased in intensity before reaching the height of the flood. The stream gauge began reading on May 19$^{th}$ with a value of 20 cfs, but the peak discharge was not until exactly three weeks later, on June 9$^{th}$ with 33,500 cfs. The greatest variance, however, still coincides with the initiation of the spring flood and is contained in the SAR image from May 27, described in Table 4.11. On this date the discharge was measured at 2,800 cfs. Given the

discharge data it stands to reason that 2005 is a thermal breakup, with temperatures causing local melting rather than a large push of water moving downstream from the headwaters in the South. Daily melting and refreezing at night would cause slush to form on top of the ice. This slushy mixture causes a large amount of backscatter leading to the high variance reported in all SAR images.

The segment rankings for 2005 display a consistent pattern pre-breakup. As seen in Table 4.12, the first three image pairs have low rank order change sums. The similarities in segment ranking of the first four images can be visually observed in Figure 4.8. Overall brightness moves up and down, but the relationship between segment ranks remains fairly consistent, with the first image set's sum of rank order change of eight, the second image set's sum of rank order change of zero, and the third a change of 2. The backscatter on the river surface (of the same river segment) had very close to the same level of intensity in consecutive pre-breakup images. The second image pair of May 9 and May 11 had a sum of rank order change of zero, indicating that backscatter brightness amongst segments maintained the exact same relationship between the two images. No discharge was recorded during this time so it can be assumed that the river surface conditions did not change between the two images. The fourth image pair (May 15 and May 27), a time period that marks the initiation of breakup, had a sum of rank order change of twelve. The change in river surface conditions is no doubt responsible for the changes in segment brightness ranking, causing some segments to appear darker as open water became more predominant, and some segments to appear brighter as ice fractured and the rough fractured surfaces backscattered incident microwaves. The actual peak discharge occurs during the next image pair, May 27 and June 13. The sum of rank order change drops to ten, just

slightly lower than in the preceding image pair but similar enough to suggest that the same processes occurring in the May 15 and May 27 image pair were likely still underway in the May 27 and June 13 image pair. The final image pair of June 13 and June 28 has a sum of rank order change of 20. This may have increased because on June 13 there was still a large volume of water moving through the channel – 16,300 cfs – but this dropped considerably to just 1,190 cfs on June 28. The drop in discharge and water depth in the channel may have caused some rapids to form near river bars and led to the increase in the sum of rank order change.

### 4.2.6 Year 2006

Results and analysis from the Lower Kuparuk River for the year 2006 are shown in Tables 4.14-4.15, and Figure 4.9.

Table 4.14: 2006 Lower Kuparuk River image information, statistics, and weather data. Date with highest variance is highlighted.

| Image Date | Variance | Stdv | Time of SAR Acquisition | Time of Weather Report | Temp (°C) | A/D | HH/VV |
|---|---|---|---|---|---|---|---|
| May 9 | 0.984 | 0.992 | 21:26 | 21:53 | -3.89 | D | VV |
| May 25 | 1.404 | 1.185 | 21:23 | 21:53 | 2.22 | D | VV |
| June 13 | 0.270 | 0.520 | 21:26 | 21:53 | 16.11 | D | VV |
| July 2 | 0.151 | 0.389 | 22:29 | 21:53 | 5 | D | VV |

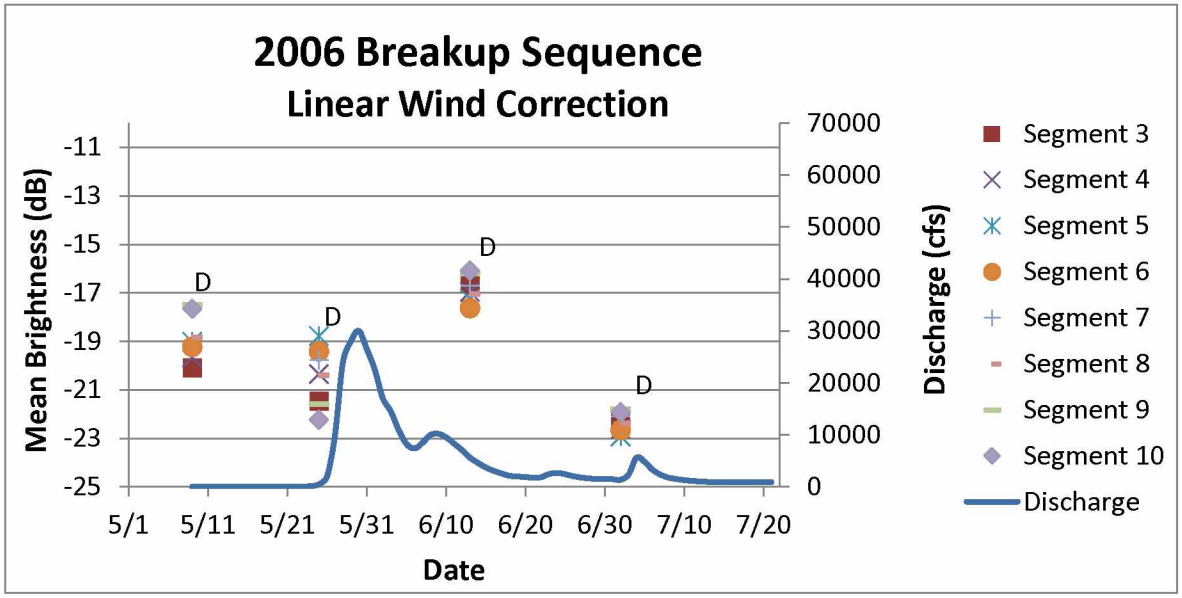


Figure 4.9: 2006 Lower Kuparuk River breakup sequence. A large variance at the initiation of breakup is clearly evident.

Table 4.15: Sum of rank order changes between river segments for 2006

| **Image Pair** | May 9/May 25 | May 25/June 13 | June 13/July 2 |
|---|---|---|---|
| **Sum of Rank Order Δ** | 26 | 30 | 8 |

2006 is another prime example of a large variance between SAR segments on an acquisition during the breakup time, as presented in Figure 4.9. The first discharge recorded is 2 cfs on May 20. The peak discharge occurs ten days later on May 30. The only SAR image taken during the breakup flood is on May 25, and it has a wide spread of mean brightness values for the different river segments. On this date the discharge recorded was 500 cfs and the variance between segments is 2.1 as recorded in Table 4.14. As seen in previous plots, there is a bright, comparatively low variance response after the flood. June 13 is the brightest overall SAR image with values ranging from -17.64 to -16.1 and a variance between segments of 0.25. The last

image in the sequence is from July 2. This image has a dark response and a low variance of 0.54. The open water present in this image reflected microwave signals away from the sensor causing the water to return a low backscatter value and have a dark signature.

The rank order analysis for 2006 does not show a pattern prior to breakup (see Table 4.15). There is a change of 26 between the first two images suggesting a change in river surface features that influenced the relative backscatter of each river segment. This increases to 30 between the next image pairs from May 25 and June 13, which is the highest sum of rank order change in the 2006 temporal series. Breakup occured between these two image acquisitions, so this high change sum can be justified by the numerous physical changes taking place at the river surface. The lowest sum of rank order change occurs in the post-breakup image pair of June 13 and July 2, suggesting that this was a time when the river was calm and conditions remained stable enough that relative backscatter between segments didn't change on a wide scale. Discharge is relatively low during both image acquisitions with 5,610 cfs on June 13 and 1,350 cfs on July 2.

### 4.2.7 Year 2007

Results and analysis from the Lower Kuparuk River for the year 2007 are shown in Tables 4.16-4.17, and Figure 4.10.

Table 4.16: 2007 Lower Kuparuk River image information, statistics, and weather data. Date with highest variance is highlighted.

| Image Date | Variance | Stdv | Time of SAR Acquisition | Time of Weather Report | Temp (°C) | A/D | HH/VV |
|---|---|---|---|---|---|---|---|
| May 14 | 0.500 | 0.707 | 07:22 | 06:53 | -12.78 | A | VV |
| May 29 | 0.163 | 0.404 | 21:26 | 21:53 | -2.22 | D | VV |
| June 1 | 0.994 | 0.997 | 21:32 | 21:53 | 0 | D | VV |
| June 5 | 0.494 | 0.703 | 03:10 | 2:53 | 2.78 | A | HH |
| June 15 | 0.198 | 0.445 | 07:16 | 6:53 | 3.89 | A | VV |

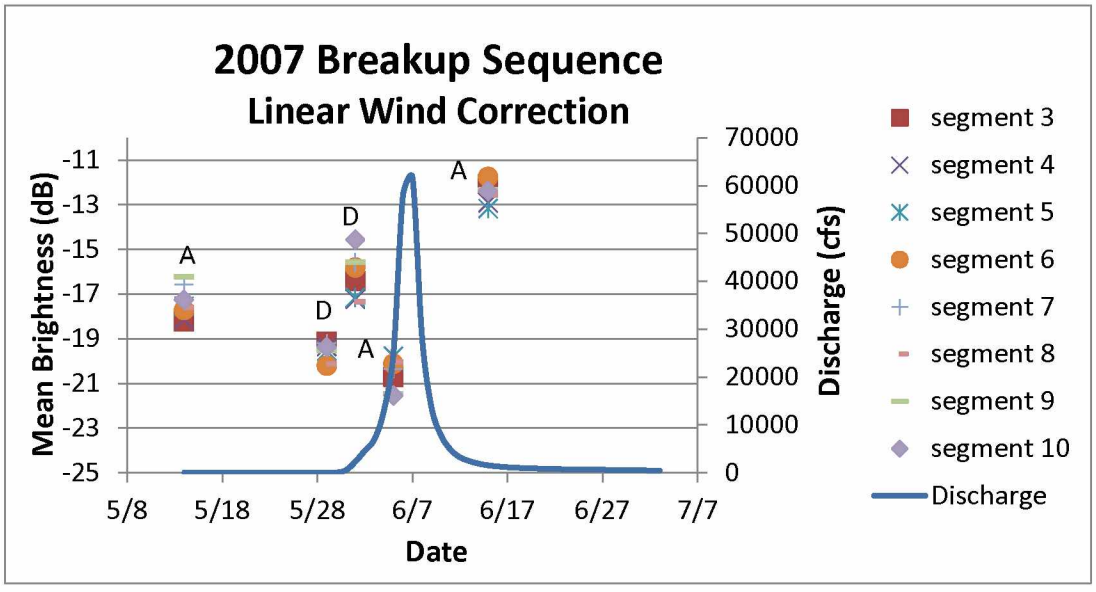


Figure 4.10: 2007 Lower Kuparuk River breakup sequence. The flood event was very short with a high discharge. The highest variance occurred on June 1.

Table 4.17: Sum of rank order changes between river segments for 2007

| **Image Pair** | May 14/May 29 | May 29/June 1 | June 1/June 5 | June 5/June 15 |
|---|---|---|---|---|
| **Sum of Rank Order Δ** | 22 | 22 | 30 | 30 |

2007 is a strong example of a mechanical breakup as evidenced by the discharge plot in Figure 4.10. The genesis of the flood was swift, moving from an initial discharge of 1 cfs on May 30, to a peak discharge of 61,700 cfs eight days later on June 7. The discharge level is impressive and double that of both 2004 and 2006, which both had discharges of 30,000 cfs. Of all the images in the 2007 season, the June 1 image has the highest variance between segments, calculated at 0.994, as recorded in Table 4.16. The discharge on this date is 2,300 cfs and is right at the beginning of the flood onset. The next image in the sequence four days later on June 5 has a smaller variance of 0.494 but is still quite high. However, this June 5 variance ranks third highest, just after the variance from the pre-breakup image on May 14 at 0.500.

Table 4.17 shows the sum of rank order changes for 2007. All the image pairs have enough changes in ranking to suggest that backscatter from the eight river segments was behaving differently in all the acquisitions with no patterns emerging between responses of individual segments. This is surprising given that there are three pre-breakup images from this year and the first breakup image, June 1, is only the third day of recorded discharge with 2,300 cfs. One interesting note is that the first two image pairs both have a sum of rank order change in rank of 22 and the last two image pairs both have a sum of rank order change of 30. The large sums of rank order change between the post-breakup image pairs may have resulted from the swift breakup flood and the tremendous drop in discharge which followed. There appear to be no

precipitation events on the hydrograph during this temporal series and a lowering of the river level could have exposed additional bars and more bank area. This would cause the backscatter at the same location along the river to vary in intensity in different SAR acquisitions throughout the spring and early summer.

### 4.2.8 Year 2008

Results and analysis from the Lower Kuparuk River for the year 2008 are shown in Tables 4.18-4.19, and Figure 4.11.

Table 4.18: 2008 Lower Kuparuk River image information, statistics, and weather data. Date with highest variance is highlighted.

| Image Date | Variance | Stdv | Time of SAR Acquisition | Time of Weather Report | Temp (°C) | A/D | HH/VV |
|---|---|---|---|---|---|---|---|
| May 13 | 0.772 | 0.879 | 21:27 | 21:53 | -3.89 | D | VV |
| May 14 | 1.017 | 1.009 | 7:20 | 6:53 | -2.78 | A | VV |
| May 16 | 0.496 | 0.705 | 21:33 | 22:53 | -1.11 | D | VV |
| June 2 | 0.197 | 0.444 | 7:23 | 6:53 | -2.78 | A | VV |
| June 17 | 0.619 | 0.787 | 21:27 | 21:53 | 15 | D | VV |

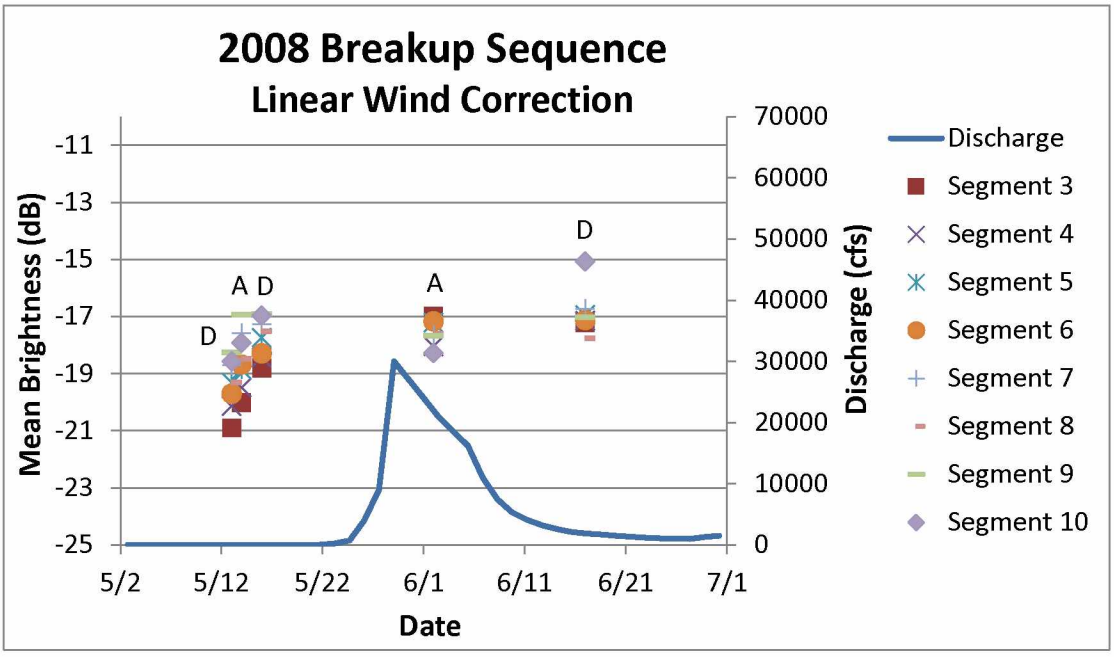


Figure 4.11: 2008 Lower Kuparuk River breakup sequence. Broad variances can be seen across all images.

Table 4.19: Sum of rank order changes between river segments for 2008

| **Image Pair** | May 13/May 14 | May 14/May 16 | May 16/June 2 | June 2/June 17 |
|---|---|---|---|---|
| **Sum of Rank Order Δ** | 4 | 4 | 26 | 26 |

There are no SAR images available during the breakup initiation of the 2008 season, and only one during the flood event was taken, as seen in Figure 4.11. A further complication in this year is the large variance present in the three pre-breakup images from May 13, 14, and 16, as presented in Table 4.18. Despite the wide array of backscatter values from the different river segments on these dates, an important feature is the relation of each segment to the same segment on different days. In all three pre-breakup images, the segments plot in a similar

pattern. Segment nine has the highest backscatter and appears bright in contrast to segment three which has the lowest mean backscatter.

The rank order analysis in Table 4.19 shows that the closely spaced image acquisitions from pre-breakup (May 13, 14, and 16) have minimal shifts in the sum of rank order changes, and this can be attributed to the presence and persistence of ice in the river that had nominal changes in surface characteristics between SAR image acquisitions. Between May 13-14 and May 14-16 the sum of rank order change is four. Visually, the similar pattern in river segment brightness response for the pre-breakup images can be seen in Figure 4.11. Between the third image pair, May 16 and June 2, breakup occurred and the sum of rank order change is quite a bit higher and rose to 26, no doubt due to the changes in backscatter as ice broke apart and was washed downstream. The low sums of rank order change calculated pre-breakup and the much higher sum of rank order change during the breakup time supports the expected trend. Post-breakup is represented by the June 2 and June 17 image pair. Here the sum of rank order change is still large, again at a value of 26. Part of this change is the result of segment ten moving from a rank of eight in the June 2 image to a rank of one in the June 17 image. It is possible that the lower water level reported by the stream gauge post-breakup (and especially in the June 17 image) caused small ripples to form on the surface of the water leading to the increase in backscatter and the change in rank order.

### 4.2.9 Year 2009

Results and analysis from the Lower Kuparuk River for the year 2009 are shown in Tables 4.20-4.21, and Figure 4.12.

Table 4.20: 2009 Lower Kuparuk River image information, statistics, and weather data. Date with highest variance is highlighted.

| Image Date | Variance | Stdv | Time of SAR Acquisition | Time of Weather Report | Temp (°C) | A/D | HH/VV |
|---|---|---|---|---|---|---|---|
| May 15 | 0.464 | 0.681 | 7:19 | 6:53 | -7.22 | A | VV |
| May 17 | 0.205 | 0.453 | 21:31 | 21:53 | 1.11 | D | VV |
| May 18 | 0.237 | 0.487 | 7:24 | 7:53 | -1.11 | A | VV |
| June 2 | 0.704 | 0.839 | 21:29 | 21:53 | 3.89 | D | VV |
| June 5 | 0.800 | 0.894 | 21:34 | 21:53 | 2.78 | D | VV |
| June 21 | 0.432 | 0.657 | 21:31 | 21:53 | 2.22 | D | VV |

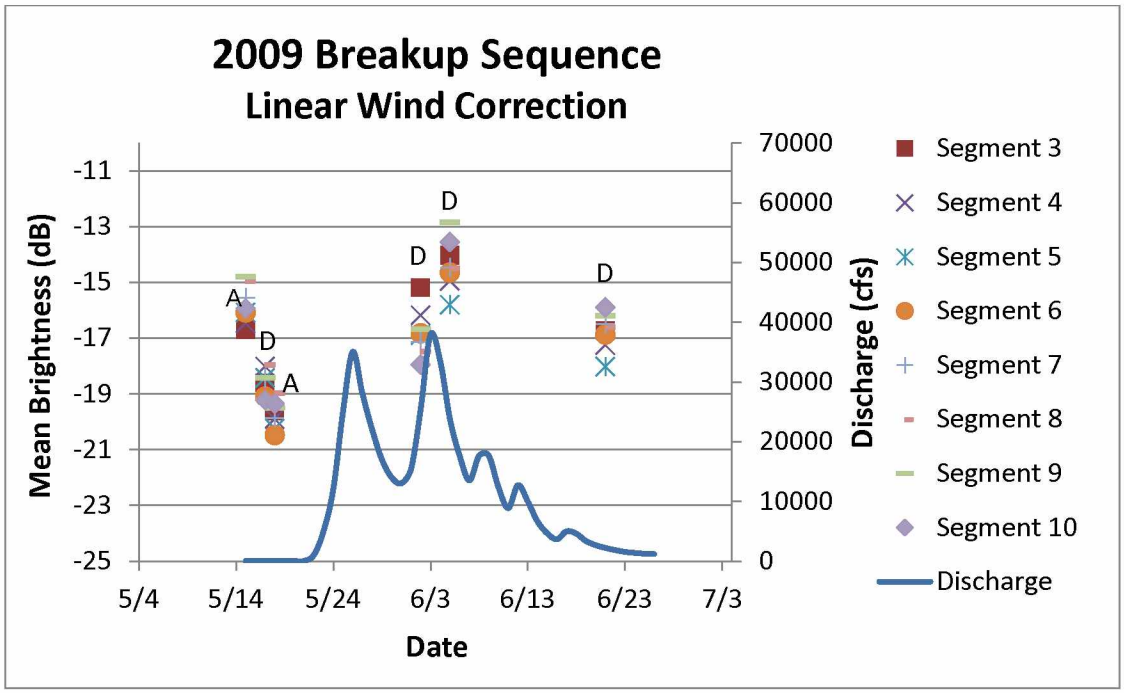


Figure 4.12: 2009 Lower Kuparuk River breakup sequence. Large variances on all days in the time series are present. Several other high discharge events occurred over the summer causing the hydrograph to have multiple curves.

Table 4.21: Sum of rank order changes between river segments for 2009

| **Image Pair** | May 15/May 17 | May 17/May 18 | May 18/June 2 | June 2/June 5 | June 5/June 21 |
|---|---|---|---|---|---|
| **Sum of Rank Order Δ** | 20 | 16 | 26 | 24 | 6 |

The hydrograph from 2009 shows two large discharge events that are closely spaced in time (Figure 4.12). It is not clear without additional field data whether these are both representing the breakup event or if the first peak is breakup and the second a separate flood event. The first peak, at 35,000 cfs occurred on May 26, just six days after the gauging station began recording. Discharge then tapered off for five days before increasing again on June 1 and reaching its highest volume on June 3 with 37,900 cfs. No SAR images were obtained during the first flood event; there was no SAR coverage from May 18 – June 2. During the second flood event,

however, two SAR images were available, one on June 2 and one on June 5. Both have large variances with 0.704 and 0.800, respectively, and are recorded in Table 4.20. Several additional, but minor flood events are seen on the hydrograph in mid-June as smaller curves. A low variance but relatively bright post-breakup image, as seen in other years, is lacking in the 2009 sequence. The last image in the series from June 21 has a moderate variance of 0.432 and plots in the middle of the dB range.

The sum of rank order change analysis presented in Table 4.21 shows a large sum of rank order change between pre-breakup and breakup image pairs. As in other years, this is surely an effect of ice being washed out of the channel. May 15 and May 17 is the first pre-breakup pair and the sum of rank order change is 20. The second pre-breakup pair is May 17 and May 18, which has a sum of rank order change of 16. This rises to 26 between the breakup image pair from May 18 and June 2. The sum of rank order changes remain high post-breakup and this may be a result of the late spring and early summer flood/high discharge events recorded in the hydrograph. Between the June 2 and June 5 image a second flood took place and the sum of rank order change was high, with a value of 24. The second flood may have been responsible for eroding away much of the bank attached snow and ice that could have been present after the first flood. However, an ice jam could also have formed between the two flood events and when it broke caused the second flood that is apparent in the stream gauge data. A Landsat image from June 9 shows the river open except for several isolated bends. If the removal of bank-attached snow from the second flood event was responsible for the differences in the sum of rank order change, this value would be high as backscatter at specific locations along the river changed dramatically with the change in snow cover. Post-breakup the sum of rank order change is fairly

stable, with a minimal sum of six. In the image pair of June 5 and June 21 the river was probably free of all ice and much of the snow around the banks leading to a consistent backscatter relationship in each river segment in both images.

### 4.2.10 Year 2010

Results and analysis from the Lower Kuparuk River for the year 2010 are shown in Tables 4.22-4.23, and Figure 4.13.

Table 4.22: 2010 Lower Kuparuk River image information, statistics, and weather data. Date with highest variance is highlighted.

| Image Date | Variance | Stdv | Time of SAR Acquisition | Time of Weather Report | Temp (°C) | A/D | HH/VV |
|---|---|---|---|---|---|---|---|
| May 18 | 0.554 | 0.744 | 21:28 | 21:53 | -2.22 | D | VV |
| May 21 | 0.348 | 0.590 | 21:33 | 21:53 | -1.11 | D | VV |
| June 4 | 0.584 | 0.764 | 7:18 | 6:53 | 30 | A | VV |
| June 6 | 0.314 | 0.561 | 21:31 | 21:53 | 2.78 | D | VV |
| June 7 | 0.285 | 0.534 | 7:24 | 7:53 | 2.22 | A | VV |
| June 22 | 0.102 | 0.319 | 21:28 | 21:53 | 2.78 | D | VV |

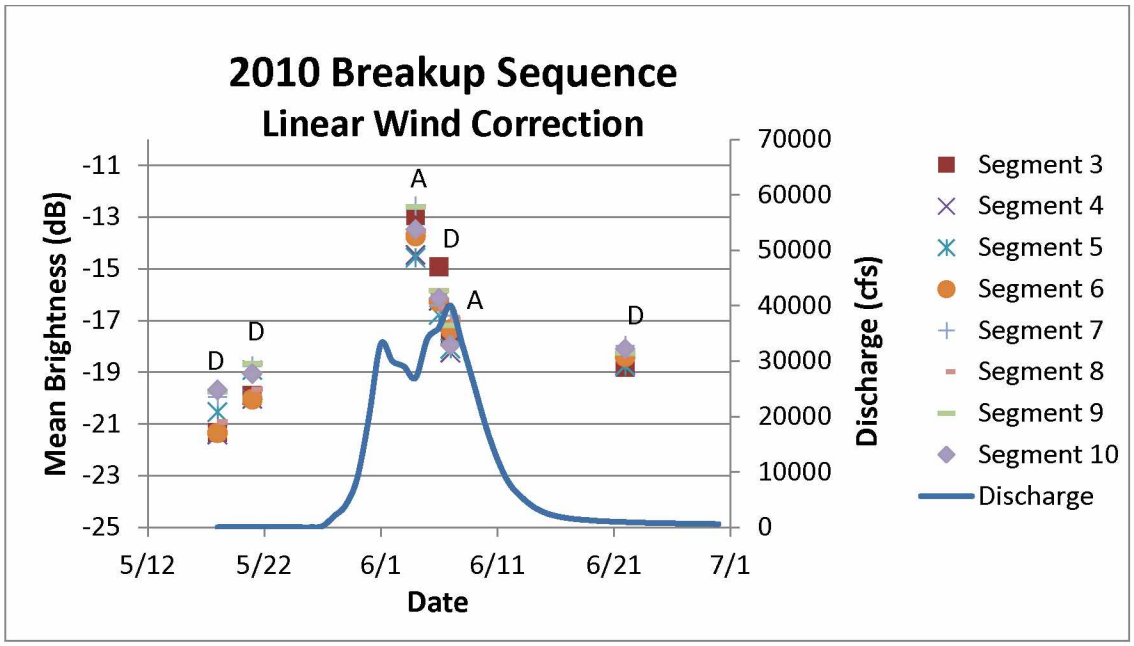


Figure 4.13: 2010 Lower Kuparuk River breakup sequence. Highest variance observed during breakup and a low variance response post-breakup.

Figure 4.23: Sum of rank order changes between river segments for 2010

| **Image Pair** | May 18/May 21 | May 21/June 4 | June 4/June 6 | June 6/June 7 | June 7/June 22 |
|---|---|---|---|---|---|
| **Sum of Rank Order Δ** | 8 | 12 | 14 | 24 | 12 |

Much like 2009, the year 2010 displays a secondary high discharge peak that is higher in volume than the initial breakup discharge, which can be viewed in Figure 4.13. Runoff is first reported on May 27 at 200 cfs. Discharge peaked on June 1 with 33,000 cfs and declined for the next three days before increasing again on June 5 and reaching a total volume of 40,000 cfs on June 7. Runoff dropped off steeply after this date. Just as in the 2009 series, no SAR imagery is available during the first discharge peak. An image from June 4 falls in between the two peaks and contains the highest variance at 0.584; variance data for all image dates is recorded in Table

4.22. Two days later, on June 6, another image was taken with a segment variance of 0.314, though this is mostly due to segment 3 plotting independently from the other segments which are closely grouped. The peak runoff date of June 7 also has a corresponding SAR image but the variance of the segments is low at 0.285. After these two hydrological events, discharge was minimal and only one other SAR image was analyzed. A June 22 image has a closely spaced, low variance signature with dB values ranging around -18.

Table 4.23 summarizes the sum of rank order change analysis. Similarities in the relationship between image segments from May 18 and May 21 can be seen in Figure 4.13. This pre-breakup image pair has a sum of rank order change of eight. The primary reason for this is the movement of segments five, nine, and ten. This is well before any recorded discharge and possibly due to winds shifting snow along the river channel in the lower half of the study area. The next image pair represents the breakup period. May 21 is pre-breakup and June 4 is during the breakup. Segments four and five shift to a lower ranking while segments three and six move to a higher ranking, with a total sum of rank order change of twelve. The increase in the sum of rank order change is a result of the transition between frozen and flood stage and supports the hypothesis that a larger sum will be inherent during breakup than pre-breakup when the river is frozen. The third image pair of June 4 and June 6 is between breakup and the second large flood event on the hydrograph. The sum of rank order change is fourteen and part of this increase in the sum may be a result of the increase in discharge. The sum of rank order change increased again to 24 between June 6 and June 7, the fourth image pair, which falls during the peak of the second runoff event on Figure 4.13 and can be accounted for by after-effects of this second flood. The

post-breakup period is represented by the fifth image pair, June 7 and June 22. Between these dates the sum of rank order change drops back down to twelve as river conditions stabilized.

### 4.3 Upper Kuparuk River

As mentioned in Section 3.4, the Upper Kuparuk River is much narrower than the Lower Kuparuk River, making it unsuitable to extract meaningful image statistics for a breakup analysis. For this part of the river only a limited visual analysis was carried out. Of the entire temporal stack from 2001 to 2010, only images from 2005 and 2006 were extracted. In the case of 2005 this was because there were two fine beam images available – one pre-breakup and one post-breakup. The year 2006 was chosen because there was a high temporal frequency of SAR images available in the archives, which allowed for a thorough analysis.

#### 4.3.1 Year 2005 Fine Beam Images

For the year 2005 two fine beam images of the Upper Kuparuk River, before and after breakup, were available. The first image was from April 15, 2005 when there was no discharge, and the second was from May 25, 2005, when discharge was measured at 130 cfs (peak discharge at the Upper Kuparuk River in 2005 was 313 cfs on May 12). Figure 4.14 shows the two images and zoomed subsets of the yellow boxes. Fine beam images have a higher spatial resolution of eight meters, which is a much higher than a standard beam SAR image, which has a spatial resolution of 25 meters. This higher resolution is sufficient to map even the narrow reaches of the Upper Kuparuk River. Unfortunately fine beam data are not acquired often enough for a detailed analysis of river surface conditions during the breakup time.

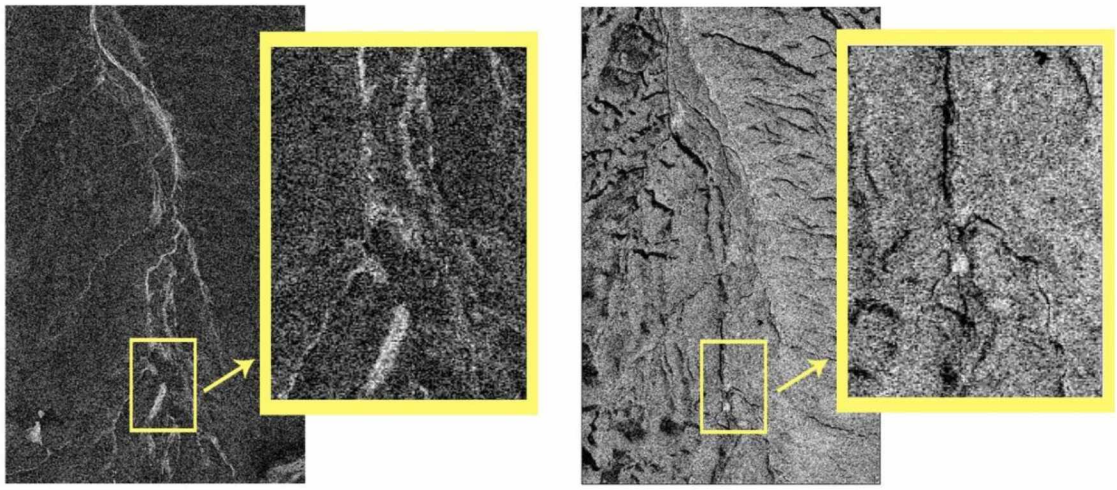


Figure 4.14: Fine beam SAR images of the Upper Kuparuk River from pre and post-breakup. At this higher resolution open water is visible in the channel on the zoomed portion of the May 25 image and appears as a dark line.

Certain key differences can be discerned from a comparison between a pre and post breakup fine beam image pair. Both images were scaled to the same minimum and maximum gray values to facilitate an unbiased comparison. In the April 15 image the background has a dark signature while the frozen river, and the snow likely to be accumulated along the river bank, shows up bright due to the high backscatter. Few changes in topography are evident due to the snow cover. The post-breakup image from May 25 is much the opposite. The river is a thin black line and the background is bright, the water was likely calm enough to serve as a specular reflector leading to the dark tone of the river. Tussocky tundra covers much of the hillsides and backscatters the incident microwaves resulting in the bright pattern. The river channel does become difficult to distinguish from the background at a few points, but is largely visible when zoomed in and guided by a polyline of the river.

### 4.3.2 Year 2006 Visual Analysis

Seventeen SAR images were analyzed between May 9, 2006 and June 25, 2006. Three were from pre-breakup when there was no river discharge, five were acquired during the breakup event (on the first curve on the hydrograph), and nine were from the post-breakup period. Nine selected subsets from this time series are shown in Figures 4.15 - 4.17. Three images from each hydrological phase (pre-breakup, breakup, and post-breakup) that were considered representative of each period are included in these figures. Discharge data from 2006 is shown in Figure 4.18 for reference.

A pattern emerged between pre-breakup and post-breakup images (Gens *et al.*, 2012). Pre-breakup, as represented by the May 9, May 13, and May 14 images in Figure 4.15, shows the river bright compared to the background, which is dark. The entire channel is clearly visible across the entire Upper Kuparuk River study area. During the breakup period, which is represented by the images from May 17, 18, and 21, (Figure 4.16) the river begins to become indistinguishable from the background. This is especially evident in the subset from May 17, which marks the second day of recorded discharge of 60 cfs at the Upper Kuparuk River. Here, the river cannot be discerned from the surrounding landscape at all except for one tiny sliver of the channel in the middle of the image, which requires zooming in to see clearly. This section appears dark and measures roughly one kilometer in length but only about one pixel in diameter. The entire subset has a brighter signature in comparison to the following image from May 18. On this day, discharge rose to 80 cfs. The May 18 subset, also displayed in Figure 4.16, shows a relatively dark background, but in the middle of the subset the river channel is visible as

a thin black line about 3.75 kilometers in length. There are a few relatively bright areas on the sides of the dark channel.

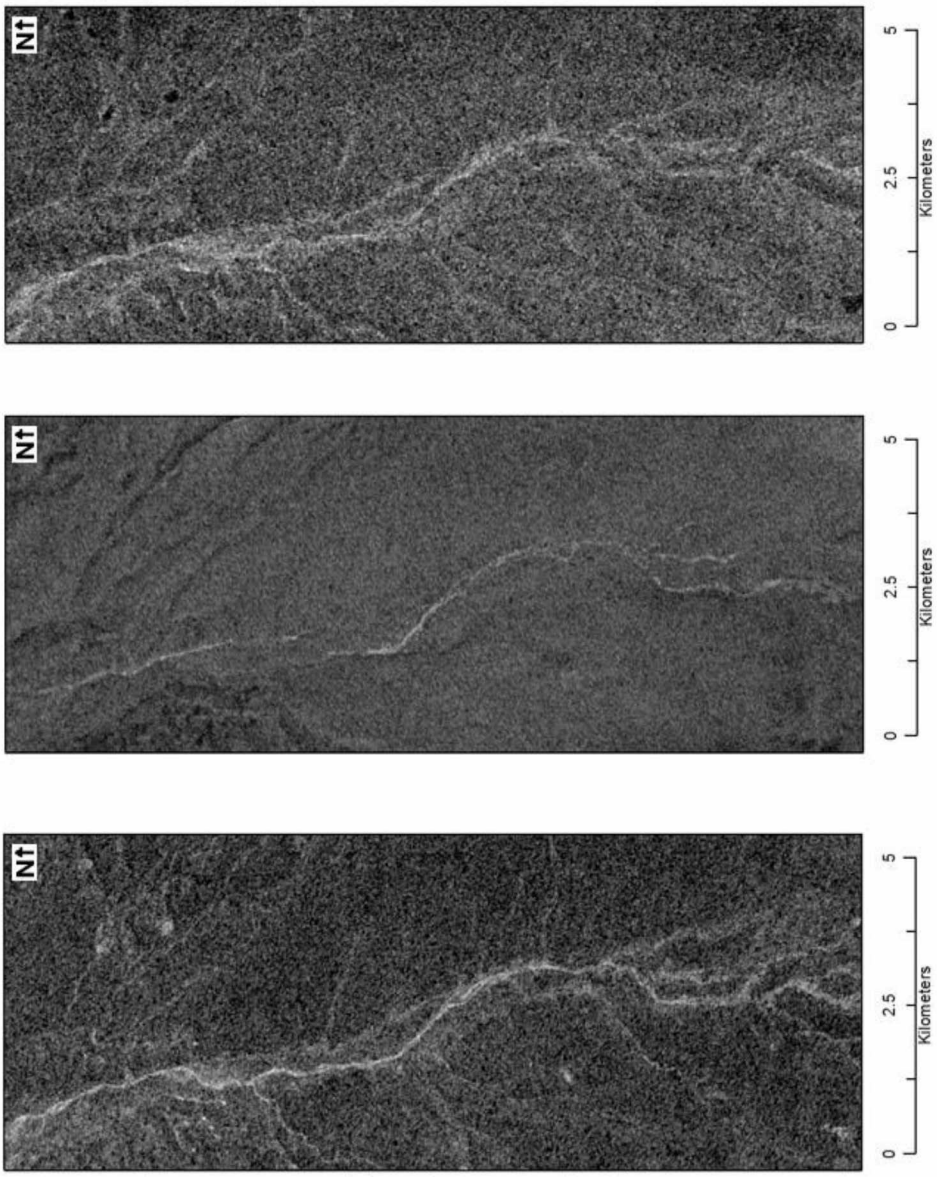


Figure 4.15: Pre-breakup Upper Kuparuk River SAR subsets. The river appears bright and the surrounding topography is dark.

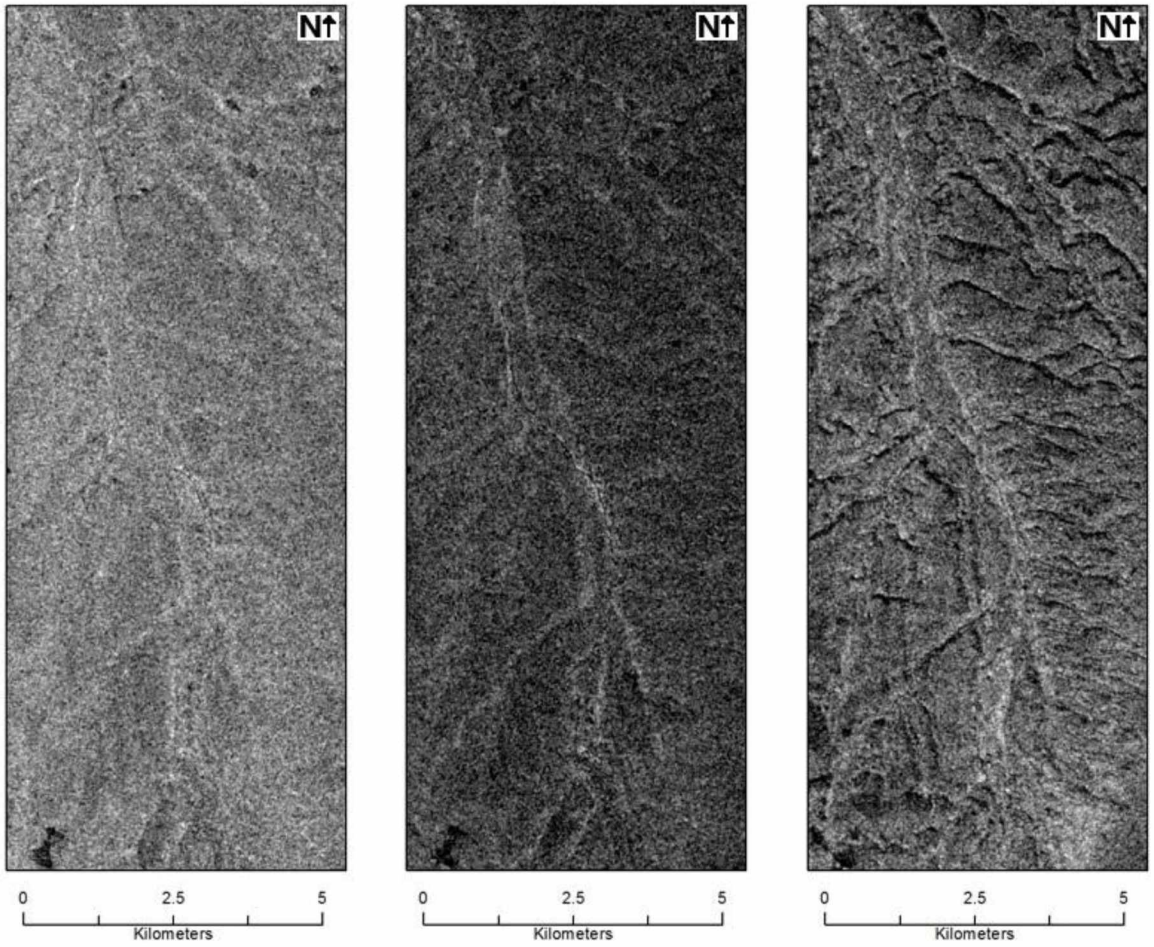


Figure 4.16: Breakup Upper Kuparuk River SAR subsets. The most notable observation from the images acquired during breakup is the lack of a clearly distinguishable river channel.

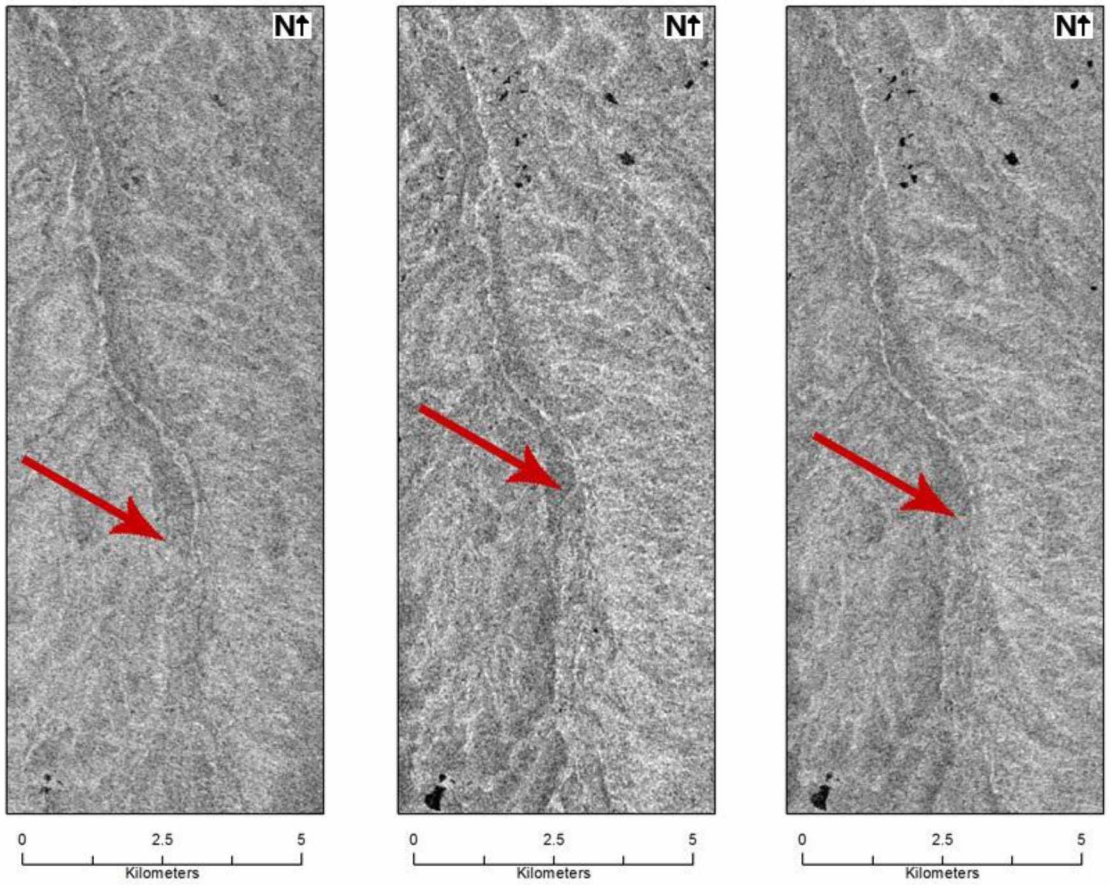


Figure 4.17: Post-breakup Upper Kuparuk River SAR subsets. Post-breakup the Southern third of the river becomes indistinguishable from the surrounding topography. This point is labeled with red arrows.

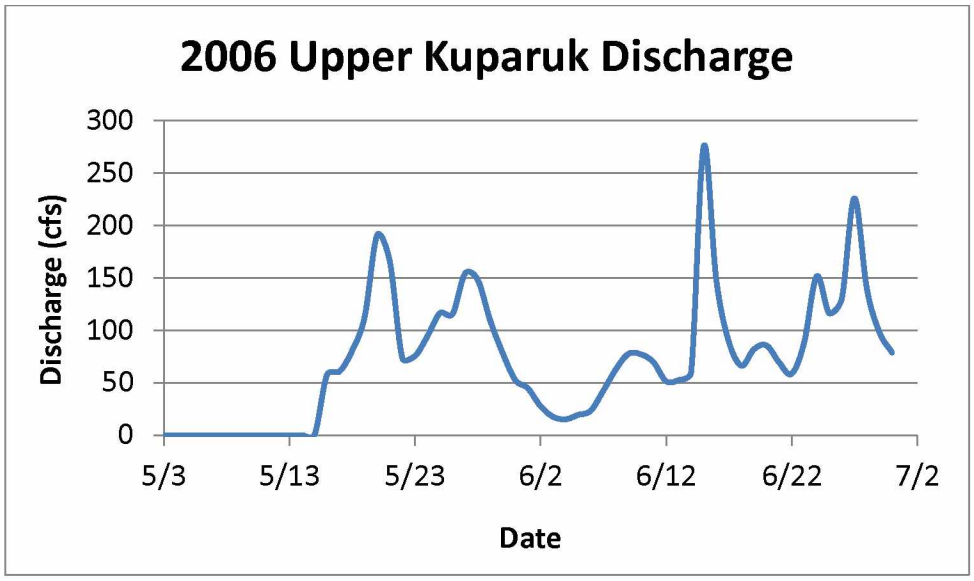


Figure 4.18: 2006 Upper Kuparuk River discharge data. Recorded by the WERC gauging station at the Upper Kuparuk River (Kane and Hinzman, 2012).

Peak discharge during the breakup flood occurred on May 20 at 190 cfs. The closest available SAR image was acquired the following day on May 21, and is also included in Figure 4.16. The May 21 image shows the background a shade of gray noticeably lighter in color than the May 18 image. The discharge was 165 cfs on May 21. The river channel looks bright in many places but a thin, dark, open channel is visible near the center of the image when zoomed in. In some places the open channel took on the appearance of a beaded stream, which looks like small ponds connected by a narrow channel. This was also noted in several of the breakup and post-breakup images not included in Figures 4.16 and 4.17.

The post-breakup phase is shown by the subsets from June 13, 17, and 20 (Figure 4.17). Discharge in all the post-breakup images is lower than images from the breakup times. June 13 had a discharge of 52 cfs. This rose to 89 cfs on June 17 and then lowered slightly to 85 cfs on

June 20. There are several noticeable observations that can be drawn from all the post-breakup images. The most obvious is that the river can be seen at the top of the subset, but the channel becomes indistinguishable from the background in the Southern third of the images. This point is labeled with red arrows on the three subsets in Figure 4.17. The second observation is that the river itself has a relatively bright signature. The channel does not appear dark post-breakup like it does in some parts of the breakup images. This may be because as the discharge lowers post-breakup, the water level also drops. Small rapids may form over rocks in the channel bed increasing the backscatter response of the river after breakup. The last notable observation from the post-breakup images is that the background landscape is bright. Unlike the pre-breakup scenes which depicted a very dark river valley, the landscape in the post-breakup imagery is much brighter. Changes in snow cover can be attributed to this shift in backscatter values.

Conclusions from the visual analysis of the 2006 Upper Kuparuk River imagery as well as overall findings at the Lower Kuparuk River are presented in Chapter 5.

## 5.0 Conclusions

### 5.1 Lower Kuparuk River Time Series Analysis and Breakup Indicators

Three variables were analyzed for defining changes during river breakup: image brightness, variance between image segments, and the sum of rank order changes between river segments pre- and post-breakup. The analysis helped to broadly bracket the breakup time for the Lower Kuparuk River for the years 2001-2010.

Table 5.1: Chart showing variables used to bracket river breakup at the Lower Kuparuk River from 2001-2010. Checks and crosses indicate whether the variables were successful indicators at bracketing the breakup event.

| Year | Brightness | Variance | Sum of Rank Order Change |
|---|---|---|---|
| 2001 | ✗ | ✓ | ✗ |
| 2002 | ✗ | N/A | N/A |
| 2003 | ✗ | ✓ | ✓ |
| 2004 | ✗ | ✓ | ✗ |
| 2005 | ✗ | ✓ | ✓ |
| 2006 | ✗ | ✓ | N/A |
| 2007 | ✗ | ✓ | ✗ |
| 2008 | ✗ | ✗ | ✓ |
| 2009 | ✗ | ✓- | ✓ |
| 2010 | ✗ | ✓ | ✗ |

Table 5.1 summarizes the overall success of each variable as a breakup indicator. Fields marked with a green fill and a ✓ represent occasions when a variable was successful as a breakup indicator, and fields marked with a red fill and a ✗ represent unsuccessful occurrences. A ✓-

with a yellow fill symbolizes a field that has debatable success. In instances where there was not enough data to carry out the analysis, the field is labeled N/A.

### 5.1.1 Image Brightness

At the start of this research it was thought that ice would nearly always backscatter heavily and open water would serve as a specular reflector and in contrast to a frozen river, look relatively dark. However, in the analyzed data, amplitude, or image brightness, went up and down, seemingly at random. Brightness fluctuated in images during the same hydrological period and, contrary to what we had imagined, was not a reliable indicator for breakup conditions in any year in the temporal series. There was no consistent change in brightness based on river surface conditions and even within one image, brightness along the channel length varied. In conclusion, image brightness is not a breakup indicator and has little applicability in discriminating between ice and open water within the Lower Kuparuk River.

### 5.1.2 Variance

Variance, as well as standard deviation (the square root of variance), between river segments was frequently elevated in images acquired during breakup compared to frozen or completely open water conditions. Variance was highest during breakup in seven of the nine years in which there was suitable data to perform the analysis. Variance did not work as a reliable breakup indicator in 2008. In 2002 there was no SAR image available during breakup. In 2008 there was a fairly high variance in all three pre-breakup images, which exceeded the variance seen in the breakup image. These high pre-breakup variances are likely due to other confounding mechanisms, such as unusual snow redistribution or possibly a slight melting of surface ice

under extended solar illumination conditions. However, we do not have reliable field data to validate this interpretation.

2009 is a somewhat controversial series. There were two flood events on the hydrograph for this year, the initial breakup flood and a second, greater flood which quickly followed. Similar to the 2002 case, there was no SAR imagery available during the first peak on the hydrograph for 2009. However, the second larger flood event does have two associated SAR images, acquired on June 2 and June 5, which have the two largest variances for that year. While it is not the breakup flood itself, it is still a flood event, and one very close to the breakup time. Theoretically, this second larger flood could have transported bank attached ice and snow that was not dislodged during the first flood event and may have resulted in the large variances. Furthermore, as the June 2 and June 5 images display high variances between segments, it still follows the hypothesis that a large variance is evident during the flood event. Therefore, this year is a conditional success and marked with a ✓⁻ symbol and a yellow fill in Table 5.1.

### 5.1.3 Sum of Rank Order Change Analysis

From the analyses of image brightness and variance we learned that the average brightness of a river segment may change significantly over time for reasons that are not related to ice breakup. Therefore, absolute image brightness is not a good measure for breakup detection. The sum of rank order change analysis is an alternate method presented and tested in this thesis for defining breakup time by analyzing relative brightness patterns along the river channel. It is assumed that these relative brightness patterns change very little pre-breakup when the frozen river ice is rather stable. During breakup where ice is shifting, fracturing, melting, and flooding,

the relative brightness patterns are expected to change dramatically. To quantify changes in brightness patterns, river segments were ranked according to their average brightness. If the brightness patterns remained unchanged between consecutive image acquisitions the rank order of segments would remain the same and the sum of rank order changes ($\mathrm{SROC} = \sum_{n=1}^{N} \Delta \mathrm{rank}_{\mathrm{segment}_n}$) will be small. If patterns change significantly, many segments will alter their position in the rank order and the sum of rank order changes will be large. To quantify whether or not the sum of rank order change analysis led to a successful bracketing of river breakup, we tried to identify significant breakup-induced increases in the sum of rank order change. For this study, an increase in the sum or rank order changes was considered significant it the change was ≥10. This was true in four years out of the time series: 2003, 2005, 2008, and 2009. These years all have at least two pre-breakup images (one pre-breakup image pair). This ranking is useful only if there is at least one pre-breakup image pair to compare to a breakup and/or post-breakup image pair. The sum of rank order change analysis could not be performed for the years 2002 and 2006 due to a lack of pre-breakup data.

### 5.2 Upper Kuparuk River Time Series Analysis

The limited width of the Upper Kuparuk River led to a visual analysis rather than a statistical analysis for investigating the break up period. The only data set that had enough spatial resolution to capture the details of in-stream characteristics was the fine beam SAR data (spatial resolution 8 meters). However, there weren't enough time sequential fine beam images to capture the pre-breakup, breakup, and post-breakup period. The visual analysis was therefore restricted to the ERS and Radarsat images. Some consistent observations related to the visual analysis of the 2005 and 2006 time series data include:

1. The full length of the channel in the Upper Kuparuk River study area was visible when the river was frozen.
2. The river was brighter compared to the background when it was frozen and when discharge was low.
3. The background topography appeared darker in pre-breakup images and a lighter gray after snowmelt.
4. During breakup and post-breakup, the southern end of the study area started to become indistinguishable from the topography.
5. On the breakup and post-breakup images, some parts of the river showed small dark patches mixed with slightly brighter regions, giving the impression of a 'beaded river'.

The transition from a river that is clearly distinguishable throughout its entire length, to a river that is not as distinguishable from the surroundings in the headwater region, was the only consistent criteria for visually bracketing the initiation of breakup in this study area. Other observations such as impressions of beaded river and higher backscatter from the surrounding tundra likely occur from processes unrelated to breakup, and therefore were not reliable indicators of breakup onset. Use of these ancillary observations for defining breakup will require further research and a much greater depth of analysis guided by field data.

### 5.3 Advantages and Limitations of Study

The analysis carried out in this study was heavily guided by field data (hydrology data from the two gauging stations). Availability of additional field data such as ice thickness and water depth would have made our understanding and analysis of the variability in the breakup process along

the river more robust. However, performing a statistical analysis of a time series of SAR data guided by the river hydrograph offers a simple and practical approach to broadly bracket the onset of the breakup period for similar Arctic rivers. This is a step-forward in the right direction.

The all-weather capability of SAR, where one is assured of data acquisition regardless of cloud cover, was the biggest advantage of using SAR for this study. Between ERS-2 and RADARSAT-1 satellites, there was enough data coverage for most of the years to generate a temporal sequence of images that was sufficient to broadly bracket the onset of breakup. A higher temporal sequence would obviously be preferable, should such frequency be available in future with launch of multiple SAR satellite systems. With a more closely spaced time sequence of image acquisitions we may be able to more precisely define the breakup period, rather than broadly bracketing it like this study does.

The use of SAR data came with limitations and complexities. The biggest limitation in this study was the low spatial resolution of the SAR sensors compared to the dimensions of the river under observation. A finer spatial resolution would have likely resulted in a more robust statistical analysis at the Lower Kuparuk River and an improved visual analysis of the Upper Kuparuk River.

The sensitivity of SAR to a variety of physical conditions and processes resulted in variable and confounding backscatter signature. The increased presence of moisture and water on the ice surface around the breakup time alters the dielectric constant, which in turn influences the backscatter response. The sensitivity of SAR to detect changes in moisture suggests that higher backscatter signatures believed to be associated with the onset of breakup may occur prior to

recorded runoff. Isolating and attributing a specific backscatter value uniquely for ice and water within the river was therefore not possible. This rendered the backscatter values alone, insignificant for this study.

### 5.4 Overall Conclusions and Recommendations

In conclusion:

- The use of SAR data has proved to be successful in bracketing the breakup period for the Lower Kuparuk River, especially for years where there was a sufficient number of SAR images available to define the pre-breakup, breakup, and post-breakup periods.
- Wind can variably affect the general backscatter values on the SAR images, sometimes causing just a slight increase and sometimes causing a significant increase in overall brightness values of the image. Therefore, a general wind correction, as proposed in this study, is recommended.
- SAR brightness (backscatter) value, or change in brightness value, in itself is not a good indicator of breakup. However, combined use of mean backscatter variance within different segments of the river, and the sum of rank order change, provides a good way to bracket the breakup period in the Lower Kuparuk River where the river is wide enough for statistical analysis.
- In areas where the river is narrow and statistical analysis is not feasible, we need to rely on visual analysis. Criteria for visually bracketing breakup are not as clear-cut as statistical methods and there is much greater dependency on field knowledge.
- River ice breakup is a highly complex process. Breakup, as determined by the hydrological community, is difficult to accurately correlate with breakup interpreted

from SAR images. SAR is very sensitive to changes in the dielectric constant as well as surface geometry and may capture changes in the surficial ice cover before any discharge is recorded on the hydrograph. This may lead to a discrepancy between defining initiation of river ice breakup using SAR versus defining the initiation using discharge data.

- For detection of river ice breakup in a similar, future study, a minimum of six images is recommended: two pre-breakup images, ideally taken within ten days of first recorded discharge, two acquisitions during the breakup event, and two post-breakup images. More images acquired within this narrow time span is preferable and will likely result in a more thorough analysis and improved determination of breakup onset.

In future, carrying out similar studies on other gauged Arctic rivers is recommended to add to the present state of knowledge. Supplementing the satellite image data sets with carefully timed airborne image acquisitions close to the breakup time will help tremendously to understand the breakup process and refine the data processing and analysis strategy for determining the breakup timing.

## References

AGDC: Alaska Geospatial Data Clearinghouse. 2012. Shapefiles: state of Alaska, Colville River, Kuparuk River, Sagavanirktok River, Dalton Highway, North Slope lakes. Last accessed August 2012.

Ashton, G.D. 1980. Freshwater ice growth, motion, and decay. In: Colbeck, S.C., ed. Dynamics of snow and ice masses. New York: Academic Press. 261-289.

Ashton, G.D. 1986. River and lake ice engineering. Littleton: Water Resources Publications. 485.

Beltaos, S. 2003. Threshold between mechanical and thermal breakup of river ice cover. Cold Regions Science and Technology 37(1):1-13, doi:10.1016/S0165-232X(03)00010-7.

Beltaos, S., Burrell, B.C., and Ismail, S. 1994. Ice and sedimentation processes in the Saint John River, Canada. In: IAHR Ice Symposium 1994, Trondheim, Norway, August 1994.

Berezovskaya, S., D. Yang, and D.L. Kane. 2004. Compatibility analysis of precipitation and runoff trends over the large Siberian watersheds. Geophysical Research Letters 31: L21502.

Best, H., McNamara, J.P., and Liberty, L. 2005. Association of ice and river channel morphology determined using ground-penetrating radar in the Kuparuk River, Alaska. Arctic, Antarctic and Alpine Research 37(2):157-162.

Bring, A., and Destouni, G. 2009. Hydrological and hydrochemical observation status in the pan-Arctic drainage basin. Polar Research 28:327-338.

Broecker, W. S. 1997. Thermohaline circulation, the Achilles Heel of our climate system: Will man-made $CO_2$ upset the current balance? Science 278:1582–1588.

Comiso, J.C., Parkinson, C.L., Gersten, R., and Stock, L. 2008. Accelerated decline in the Arctic sea ice cover. Geophysical Research Letters 33, L01703, doi:10.1029/2007GL031972.

Delaney, A., Arcone, S. and Chacho Jr., E. 1990. Winter short-pulse radar studies on the Tanana River, Alaska. Arctic 43:244-250.

Déry S.J., Stieglitz, M., Rennermalm, A.K., and Wood, E.F. 2005. The water budget of the Kuparuk River Basin, Alaska. Journal of Hydrometeorology 6:633-655, doi:10.1175/JHM434.1.

Ferrick, M.G., and Mulherin, D. 1989. Framework for Control of Dynamic Ice Breakup by River Regulation. CRREL Report 89-2. US Army Cold Regions and Engineering Laboratory, Springfield.

Floyd, A., Liljedahl, A.K., Gens, R., Prakash, A., and Mann, D.H. 2011. Remote Sensing, modeling, and in-situ measurements to study the spring and summer thermal regime of the Kuparuk River, Northern Alaska. Trans. American Geophysical Union 92(52), Fall Meeting Supplementary. Abstract no. C41C-0422.

Floyd, A., Liljedahl, A.K., Prakash, A., Gens, R., and Meyer, F. 2012. Using synthetic aperture radar to study river ice breakup on the Kuparuk River, Northern Alaska. American Water Resource Association Alaska Section Annual Conference, March 5-7, Juneau, Alaska.

Gens, R. 2008. SAR: Principles and Applications. Lecture Notes.

Gens, R. and Logan, T. 2003. Alaska Satellite Facility software tools: Manual. Geophysical Institute, UAF, ISBN 0-915360-16-0, 180 pages.

Gens, R., Wirth, L., Floyd, A., and Barker, E. 2012. Using of SAR imagery for open water characterization in cold northern climates. IEEE International Geoscience and Remote Sensing Symposium, Munich, Germany.

Gerard, R. 1983. River and lake ice processes relevant to ice loads. In: Caldwell, S.R., and Crissman, R.D., eds. Design for Ice Forces. New York: American Society of Civil Engineers. 121-138.

Hanssen, R.F. 2001. Radar interferometry: Data interpretation and analysis. Dordrecht: Kluwer Academic Publishers. 308 p.

Hastings, S.J., Luchessa, S.A., Oechel, W.C., and Tenhunen, J.D. 1989. Standing biomass and production in water drainages of the foothills of the Phillip Smith Mountains. Holarctic Ecology 12(3):304-311.

Hinzman, L.D., Bettez, N.D., Bolton, W.R., Chapin, F.S., Dyurgerov, M.B., Fastie, C.L., Griffith, B., et al. 2005. Evidence and implications of recent climate change in northern Alaska and other arctic regions. Climatic Change 72:251-298.

Hinzman, L.D., Gieck, R.E., and Kane, D.L. 2008. Spatial and temporal variation of soil temperatures and Arctic hydrology in the Kuparuk River basin, Alaska. International Conference on Permafrost (ICOP) Proceedings (9):711-716.

Holland, M., Bitz, C., and Tremblay, B. 2006. Future abrupt reduction in the summer Arctic sea ice. Geophysical Research Letters 33, L23503.

Horstmann, J., Schiller, H., Schulz-Stellenfleth, J., and Lehner, S. 2003. Global wind speed retrieval from SAR. IEEE Transactions on Geoscience and Remote Sensing 41(10):2277-2286.

Hubbard, R.J., Edrich, S.P., and Rattey, R.P. 1987. Geologic evolution and hydrocarbon habitat of the 'Arctic Alaska Microplate'. Marine and Petroleum Geology 4:2-34.

Kane, D.L., and Hinzman, L.D. 2012. Climate data from the North Slope Hydrology Research project. University of Alaska Fairbanks, Water and Environmental Research Center. URL: http://ine.uaf.edu/werc/projects/NorthSlope/upper_kuparuk/uk_river/uk_river.html. Fairbanks: University of Alaska Fairbanks. Last accessed April 2012.

Kane, D.L., Hinzman, L.D., Benson, C.S., and Liston, G.E. 1991. Snow hydrology of a headwater Arctic Basin. 1. Physical measurements and process studies. Water Resources Research 27(6):1099-1109.

Kane, D.L., Gieck, R.E., and Hinzman, L.D. 1997. Snowmelt modeling at small Alaskan Arctic watershed. Journal of Hydrologic Engineering 2(4):204-2010.

Kane, D.L., Soden, D.J., Hinzman, L.D., Gieck, R.E. 1998. Rainfall runoff of a nested watershed in the Alaskan Arctic. Proceedings of the Seventh International Conference on Permafrost, Yellowknife, NT, Canada, Université Laval, 539-543.

Kane, D.L., Hinzman, L.D., McNamara, J.P., Zhang, Z., and Benson, C.S. 2000. An overview of a nested watershed study in Arctic Alaska. Nordic Hydrology 31:245-266.

Kane, D.L., McNamara, J.P., Yang, D., Olsson, P.Q., and Gieck, R.E. 2003. An extreme rainfall/runoff event in Arctic Alaska. Journal of Hydrometeorology 4:1220-1228.

Kane, D.L., Hinzman, L.D., Gieck, R.E., McNamara, J.P., Youcha, E.K., and Oatley, J.A. 2008. Contrasting extreme runoff events in areas of continuous permafrost, Arctic Alaska. Hydrology Research 39(4):287-298, doi:10.2166/nh.2008.005.

Liljedahl, A.K., Hinzman, L.D., Harazono, Y., Zona, D., Tweedie, C.E., Hollister, R.D., Engstrom, R., Oechel, W.C. 2011. Nonlinear controls on evapotranspiration in arctic coastal wetlands. Biogeosciences 8: 3375-3389, doi:10.5194/bg-8-3375-2011.

Lillesand, T.M., Kiefer, R.W., and Chipman, J.W. 2008. Remote sensing and image interpretation (6th ed.). New York: John Wiley & Sons. 756 p.

Martini, I.P., Kwong, J.K., and Sadura, S. 1993. Sediment ice rafting and cold climate fluvial deposits: Albany River, Ontario, Canada. Special Publication of the International Association of Sedimentologists 17:63-76.

McNamara, J.P., Kane, D.L., and Hinzman, L.D. 1998. An analysis of streamflow hydrology in the Kuparuk River Basin, Arctic Alaska: A nested watershed approach. Journal of Hydrology 206:39-57.

McNamara, J.P., Kane, D.L., and Hinzman, L.D. 1999. An analysis of an arctic channel network using a digital elevation model. Geomorphology 29:339-353.

Mermoz, S., Allain, S., Bernier, M., and Pottier, E. 2008. River ice mapping from polsar images. Geoscience and Remote Sensing Symposium, 2008. 3:23-26.

Michel, B. 1978. Ice mechanics. Quebec City: Les Presses de l'Universite Laval. 499 p.

Michel, B., and Drouin, M. 1972. Formation, classification et proprietes mecaniques de la glace. Sixieme colloque d'initiation aux principes de l'hydrologie. Report GCE-72-08-01. 18 p.

Michel, B. and Ramseier, R.O. 1971. Classification of river and lake ice. Canadian Geotechnical Journal 8:36-45.

Muller, S.V., Walker, D.A., Nelson, F.E., Auerbach, N.A., Bockheim, J.G., Guyer, S., and Sherba, D. 1998. Accuracy assessment of the land-cover map of the Kuparuk River Basin, Alaska: Considerations for remote regions. Photogrammetric Engineering & Remote Sensing 64(6): 619-628.

Nelson, F.E., Shiklomanov, N.I., Mueller, G.R., Hinkel, K.M., Walker, D.A., and Bockheim, J.G. 1997. Estimating active-layer thickness over a large region: Kuparuk River Basin, Alaska, U.S.A. Arctic and Alpine Research 29(4): 367-378.

Niehus, C.A. 2002. Evaluation of factors affecting ice forces at selected bridges in South Dakota. Water Resources Investigations Report 02-4158. U.S. Department of the Interior, U.S. Geological Survey, Denver.

Osterkamp, T.E. 1975. Observations on Tanana River ice. In: IAHR, Proceedings, Third International Symposium on Ice Problems, held 18-21 August 1975, Hanover, New Hampshire. 201-208.

Osterkamp, T.E., and Payne, M.W. 1981. Estimates of permafrost thickness from well logs in northern Alaska. Cold Region Science and Technology 5(1): 13-27.

Peterson, B. J., Holmes, R. M., McClelland, J.W., Vörösmarty, C. J., Lammers, R. B., Shiklomanov, A. I., Shiklomanov, I. A., and Rahmstorf, S. 2002. Increasing river discharge to the Arctic Ocean. Science 298:2171–2173.

Rahmstorf, S. 2002. Ocean circulation and climate during the past 120,000 years. Nature 419:207-214.

Rovansek, R.J., Hinzman, L.D., and Kane, D.L. 1996. Hydrology of a tundra wetland complex on the Alaskan Arctic Coastal Plain, USA. Arctic and Alpine Research 28(3):311-317.

Savelieva, N. I., Semiletov, I. P., Vasilevskaya, L. N., and Pugach, S. P. (2000) A climate shift in seasonal values of meteorological and hydrological parameters for Northeastern Asia. Progress in Oceanography, 47:279–297.

Searcy, C., Dean, K., and Stringer, W. 1996. A river-coastal sea ice interaction model: Mackenzie River Delta. Journal of Geophysical Research 101(C4):8885, doi:10.1029/96JC00120

Shiklomanov, N.I., and Nelson, F.E. 2002. Active-layer mapping at regional scales: a 13-year spatial time series for the Kuparuk Region, North-Central Alaska. Permafrost and Periglacial Processes 13(3):219-230, doi:10.1002/ppp.425.

Siegle, D. 2012. Critical values of the Pearson Product-Moment Correlation Coefficient. URL: http://www.gifted.uconn.edu/siegle/research/Correlation/corrchrt.htm. Storrs, Connecticut. Last accessed June 12, 2012.

Smith, D.G. 1980. River ice processes: thresholds and geomorphologic effects in northern and mountain rivers. In: Coates, D.R., and Vitek, J.D., eds. Thresholds in geomorphology. London: George Allen and Unwin. 323-343.

Steele, M., Thomas, D., and Rothrock, D. 1996. A simple model study of the Arctic Ocean freshwater balance, 1979-1985. Journal of Geophysical Research 101(NC9):20833-20848.

Stroeve, J., Serreze, M., Drobot, S., Gearheard, S., Holland, M., Maslanik, J., Meier, W., Scambos, T. 2008. Arctic sea ice extent plummets in 2007. Eos, Transactions of the American Geophysical Union 89:13-14, doi:10.1029/2008EO020001.

Toolik Field Station. 2012. Toolik Field Station Spatial Data. Fairbanks: University of Alaska Fairbanks. http://toolik.alaska.edu/gis/data/index.php. Last accessed August 2012.

Trochim, E., Prakash, A., and Kane, D. 2010a. Capturing water tracks using remote sensing in the foothills of the Alaskan Arctic: a multi-data perspective. Alaska Section AWRA Annual Conference, March 31-April 2, Anchorage, Alaska.

Trochim, E., Prakash, A., and Kane, D. 2010b. Assessing the impacts of the hydrological drainage networks upon the characteristics of permafrost in the Upper Kuparuk region. Third European Conference on Permafrost, June 13-17, Svalbard, Norway.

Tsang, G. 1982. Frazil and anchor ice: A monograph. National Research Council of Canada, Subcommittee on Hydraulics of Ice-covered Rivers, Ottawa, 89 p.

Unterschultz, K.D., van der Sanden, J., and Hicks, F.E. 2009. Potential of RADARSAT-1 for the monitoring of river ice: Results of a case study on the Athabasca River at Fort McMurray, Canada. Cold Regions Science and Technology 55:238-248.

USGS. 2012. USGS 15896000 Kuparuk River Near Deadhorse, AK. http://waterdata.usgs.gov/nwis/nwisman/?site_no=15896000&agency_cd=USGS. Last accessed June 2012.

Walker, M.D., Walker, D.A., and Everett, K.R. 1989. Wetland soils and vegetation, Arctic Foothills, AK. US Department of the Interior Biological Report 89 (7).

Wang, M. and Overland, J.E. 2009. A sea ice free summer Arctic within 30 years? Geophysical Research Letters 36, L07502.

Weber, F., Nixon, D., and Hurley, J. 2003. Semi-automated classification of river ice types on the Peace River using RADARSAT-1 synthetic aperture radar (SAR) imagery. Canadian Journal of Civil Engineering 30: 11-27, doi: 10.1139/L02-073.

Williams, G.P., and Mackay, D.K. 1973. The characteristics of ice jams. In: Williams, G.P., ed. Seminar on Ice Jams in Canada. Technical Memorandum 107. National Research Council of Canada, Associate Committee on Geotechnical Research, Ottawa. 17-35.

Woodhouse, I.H. 2006. Introduction to Microwave Remote Sensing. Boca Raton: Taylor and Francis Group. 370 p.

Yang, D., Kane, D. L., Hinzman, L. D., Zhang, X., Zhang, T., and Ye, H. (2002) Siberian Lena River hydrologic regime and recent change, Journal of Geophysical Research 107(D23): 4694.

Yoshikawa, K., Hinzman, L. D., and Kane, D. L. 2007. Spring and aufeis (icing) hydrology in Brooks Range, Alaska. Journal of Geophysical Research 112: G04S43, doi:10.1029/2006JG000294.

Zachrisson, G. 1988. Reduction of damages from ice jam flooding in River Tornealven. In: Laasanen, O. and Forsius, J., eds. IAHR, Proceedings of the Nordic Expert Meeting on River Ice. Helsinki: Nordic Hydrological Programme Report No. 21: 217-225.

Zhang, T., Osterkamp, T.E., and Stamnes, K. 1996. Some characteristics of the climate in Northern Alaska, USA. Arctic and Alpine Research 28(4):509-518.

# Appendices

## Appendix A: Lower Kuparuk River Discharge Data

Table A-1: 2001 Lower Kuparuk River discharge data. USGS station ID number 15896000. Day of peak discharge is highlighted.

| 2001 Lower Kuparuk River Discharge Data | | | | |
|---|---|---|---|---|
| **Date** | **Cfs** | | **Date** | **Cfs** |
| 5/29 | 0 | | 6/18 | 6480 |
| 5/31 | 0 | | 6/19 | 5070 |
| 6/1 | 0 | | 6/20 | 3970 |
| 6/2 | 0 | | 6/21 | 3260 |
| 6/3 | 0 | | 6/22 | 2760 |
| 6/4 | 0 | | 6/23 | 2460 |
| 6/5 | 0 | | 6/24 | 2550 |
| 6/6 | 1000 | | 6/25 | 2770 |
| 6/7 | 4000 | | 6/26 | 2590 |
| 6/8 | 12000 | | 6/27 | 2230 |
| 6/9 | 38000 | | 6/28 | 1870 |
| 6/10 | 55000 | | 6/29 | 1650 |
| 6/11 | 43000 | | 6/30 | 1910 |
| 6/12 | 30000 | | 7/1 | 2370 |
| 6/13 | 22200 | | 7/2 | 2160 |
| 6/14 | 16500 | | 7/3 | 1770 |
| 6/15 | 12100 | | 7/4 | 1510 |
| 6/16 | 9820 | | 7/5 | 1320 |
| 6/17 | 8270 | | | |

Table A-2: 2002 Lower Kuparuk River discharge data. USGS station ID number 15896000. Day of peak discharge is highlighted.

| 2002 Lower Kuparuk River Discharge Data | | | | | |
|---|---|---|---|---|---|
| **Date** | **Cfs** | **Date** | **Cfs** | **Date** | **Cfs** |
| 5/3 | 0 | 5/26 | 36000 | 6/18 | 2050 |
| 5/4 | 0 | 5/27 | 18100 | 6/19 | 1700 |
| 5/5 | 0 | 5/28 | 10600 | 6/20 | 1410 |
| 5/6 | 0 | 5/29 | 7790 | 6/21 | 1130 |
| 5/7 | 0 | 5/30 | 6510 | 6/22 | 990 |
| 5/8 | 0 | 5/31 | 4800 | 6/23 | 992 |
| 5/9 | 0 | 6/1 | 4380 | 6/24 | 1560 |
| 5/10 | 0 | 6/2 | 4580 | 6/25 | 4080 |
| 5/11 | 0 | 6/3 | 4070 | 6/26 | 4670 |
| 5/12 | 0 | 6/4 | 3310 | 6/27 | 3700 |
| 5/13 | 0 | 6/5 | 3120 | 6/28 | 2940 |
| 5/14 | 0 | 6/6 | 3210 | 6/29 | 2500 |
| 5/15 | 0 | 6/7 | 3250 | 6/30 | 2600 |
| 5/16 | 0 | 6/8 | 2750 | 7/1 | 3340 |
| 5/17 | 0 | 6/9 | 2350 | 7/2 | 3430 |
| 5/18 | 0 | 6/10 | 1920 | 7/3 | 3610 |
| 5/19 | 0 | 6/11 | 1640 | 7/4 | 3750 |
| 5/20 | 0 | 6/12 | 1450 | 7/5 | 3490 |
| 5/21 | 500 | 6/13 | 1250 | 7/6 | 3210 |
| 5/22 | 5000 | 6/14 | 1100 | 7/7 | 2760 |
| 5/23 | 25000 | 6/15 | 1000 | 7/8 | 2410 |
| 5/24 | 50000 | 6/16 | 1280 | 7/9 | 2720 |
| 5/25 | 45000 | 6/17 | 2030 | | |

Table A-3: 2003 Lower Kuparuk River discharge data. USGS station ID number 15896000. Day of peak discharge is highlighted.

| 2003 Lower Kuparuk River Discharge Data | | | | |
|---|---|---|---|---|
| **Date** | **Cfs** | | **Date** | **Cfs** |
| 5/4 | 0 | | 6/1 | 500 |
| 5/5 | 0 | | 6/2 | 2000 |
| 5/6 | 0 | | 6/3 | 4000 |
| 5/7 | 0 | | 6/4 | 9000 |
| 5/8 | 0 | | 6/5 | 20000 |
| 5/9 | 0 | | 6/6 | 38000 |
| 5/10 | 0 | | 6/7 | 43000 |
| 5/11 | 0 | | 6/8 | 31400 |
| 5/12 | 0 | | 6/9 | 21400 |
| 5/13 | 0 | | 6/10 | 16500 |
| 5/14 | 0 | | 6/11 | 12100 |
| 5/15 | 0 | | 6/12 | 9150 |
| 5/16 | 0 | | 6/13 | 7090 |
| 5/17 | 0 | | 6/14 | 5780 |
| 5/18 | 0 | | 6/15 | 4900 |
| 5/19 | 0 | | 6/16 | 4330 |
| 5/20 | 0 | | 6/17 | 3950 |
| 5/21 | 0 | | 6/18 | 3630 |
| 5/22 | 0 | | 6/19 | 3320 |
| 5/23 | 0 | | 6/20 | 3000 |
| 5/24 | 0 | | 6/21 | 2760 |
| 5/25 | 0 | | 6/22 | 2490 |
| 5/26 | 0 | | 6/23 | 2190 |
| 5/27 | 0 | | 6/24 | 1930 |
| 5/28 | 0 | | 6/25 | 1780 |
| 5/29 | 0 | | 6/26 | 1650 |
| 5/30 | 10 | | 6/27 | 1550 |
| 5/31 | 100 | | | |

Table A-4: 2004 Lower Kuparuk River discharge data. USGS station ID number 15896000. Day of peak discharge is highlighted.

| 2004 Lower Kuparuk River Discharge Data | | | | | |
|---|---|---|---|---|---|
| **Date** | **Cfs** | **Date** | **Cfs** | **Date** | **Cfs** |
| 5/7 | 0 | 5/30 | 22000 | 6/22 | 2020 |
| 5/8 | 0 | 5/31 | 24000 | 6/23 | 1810 |
| 5/9 | 0 | 6/1 | 26000 | 6/24 | 1680 |
| 5/10 | 0 | 6/2 | 28000 | 6/25 | 1570 |
| 5/11 | 0 | 6/3 | 30000 | 6/26 | 1550 |
| 5/12 | 0 | 6/4 | 29000 | 6/27 | 1490 |
| 5/13 | 0 | 6/5 | 26500 | 6/28 | 1630 |
| 5/14 | 0 | 6/6 | 24600 | 6/29 | 1730 |
| 5/15 | 0 | 6/7 | 19400 | 6/30 | 1550 |
| 5/16 | 0 | 6/8 | 16000 | 7/1 | 1370 |
| 5/17 | 0 | 6/9 | 12900 | 7/2 | 1270 |
| 5/18 | 0 | 6/10 | 9370 | 7/3 | 1170 |
| 5/19 | 10 | 6/11 | 7110 | 7/4 | 1090 |
| 5/20 | 50 | 6/12 | 5910 | 7/5 | 1040 |
| 5/21 | 300 | 6/13 | 5220 | 7/6 | 1010 |
| 5/22 | 1000 | 6/14 | 4960 | 7/7 | 1020 |
| 5/23 | 1800 | 6/15 | 4570 | 7/8 | 1020 |
| 5/24 | 3000 | 6/16 | 4000 | 7/9 | 1250 |
| 5/25 | 5000 | 6/17 | 3600 | 7/10 | 2410 |
| 5/26 | 8000 | 6/18 | 3370 | 7/11 | 3070 |
| 5/27 | 11000 | 6/19 | 2890 | 7/12 | 5610 |
| 5/28 | 15000 | 6/20 | 2590 | 7/13 | 8340 |
| 5/29 | 19000 | 6/21 | 2310 | 7/14 | 6440 |

Table A-5: 2005 Lower Kuparuk River discharge data. USGS station ID number 15896000. Day of peak discharge is highlighted.

| 2005 Lower Kuparuk River Discharge Data | | | | | |
|---|---|---|---|---|---|
| **Date** | **Cfs** | **Date** | **Cfs** | **Date** | **Cfs** |
| 5/8 | 0 | 6/1 | 9000 | 6/25 | 1520 |
| 5/9 | 0 | 6/2 | 9400 | 6/26 | 1410 |
| 5/10 | 0 | 6/3 | 10000 | 6/27 | 1290 |
| 5/11 | 0 | 6/4 | 11500 | 6/28 | 1190 |
| 5/12 | 0 | 6/5 | 14000 | 6/29 | 1120 |
| 5/13 | 0 | 6/6 | 19700 | 6/30 | 1070 |
| 5/14 | 0 | 6/7 | 29500 | 7/1 | 1020 |
| 5/15 | 0 | 6/8 | 32100 | 7/2 | 1000 |
| 5/16 | 0 | 6/9 | 33500 | 7/3 | 1050 |
| 5/17 | 0 | 6/10 | 32200 | 7/4 | 1030 |
| 5/18 | 0 | 6/11 | 26100 | 7/5 | 999 |
| 5/19 | 20 | 6/12 | 21300 | 7/6 | 1020 |
| 5/20 | 40 | 6/13 | 16300 | 7/7 | 1000 |
| 5/21 | 80 | 6/14 | 12300 | 7/8 | 1010 |
| 5/22 | 200 | 6/15 | 11000 | 7/9 | 1020 |
| 5/23 | 400 | 6/16 | 11300 | 7/10 | 1130 |
| 5/24 | 700 | 6/17 | 9010 | 7/11 | 1230 |
| 5/25 | 1200 | 6/18 | 6760 | 7/12 | 1690 |
| 5/26 | 1800 | 6/19 | 5530 | 7/13 | 3380 |
| 5/27 | 2800 | 6/20 | 4390 | 7/14 | 3820 |
| 5/28 | 4300 | 6/21 | 3360 | 7/15 | 3590 |
| 5/29 | 6000 | 6/22 | 2640 | 7/16 | 2980 |
| 5/30 | 7200 | 6/23 | 2160 | 7/17 | 2250 |
| 5/31 | 8300 | 6/24 | 1760 | | |

Table A-6: 2006 Lower Kuparuk River discharge data. USGS station ID number 15896000. Day of peak discharge is highlighted.

| 2006 Lower Kuparuk River Discharge Data | | | | | |
|---|---|---|---|---|---|
| **Date** | **Cfs** | **Date** | **Cfs** | **Date** | **Cfs** |
| 5/9 | 0 | 6/3 | 14600 | 6/28 | 1610 |
| 5/10 | 0 | 6/4 | 11000 | 6/29 | 1510 |
| 5/11 | 0 | 6/5 | 8250 | 6/30 | 1500 |
| 5/12 | 0 | 6/6 | 7370 | 7/1 | 1450 |
| 5/13 | 0 | 6/7 | 8430 | 7/2 | 1350 |
| 5/14 | 0 | 6/8 | 9940 | 7/3 | 2390 |
| 5/15 | 0 | 6/9 | 10200 | 7/4 | 5620 |
| 5/16 | 0 | 6/10 | 9510 | 7/5 | 4800 |
| 5/17 | 0 | 6/11 | 8310 | 7/6 | 3290 |
| 5/18 | 0 | 6/12 | 7050 | 7/7 | 2340 |
| 5/19 | 0 | 6/13 | 5610 | 7/8 | 1770 |
| 5/20 | 2 | 6/14 | 4610 | 7/9 | 1490 |
| 5/21 | 4 | 6/15 | 3710 | 7/10 | 1290 |
| 5/22 | 10 | 6/16 | 3060 | 7/11 | 1130 |
| 5/23 | 40 | 6/17 | 2550 | 7/12 | 1030 |
| 5/24 | 150 | 6/18 | 2120 | 7/13 | 938 |
| 5/25 | 500 | 6/19 | 1980 | 7/14 | 877 |
| 5/26 | 2000 | 6/20 | 1870 | 7/15 | 840 |
| 5/27 | 10000 | 6/21 | 1740 | 7/16 | 843 |
| 5/28 | 24000 | 6/22 | 1860 | 7/17 | 846 |
| 5/29 | 28000 | 6/23 | 2460 | 7/18 | 848 |
| 5/30 | 30000 | 6/24 | 2640 | 7/19 | 861 |
| 5/31 | 26500 | 6/25 | 2420 | 7/20 | 840 |
| 6/1 | 22600 | 6/26 | 2050 | 7/21 | 882 |
| 6/2 | 17100 | 6/27 | 1780 | | |

Table A-7: 2007 Lower Kuparuk River discharge data. USGS station ID number 15896000. Day of peak discharge is highlighted.

| 2007 Lower Kuparuk River Discharge Data | | | |
|---|---|---|---|
| **Date** | **cfs** | **Date** | **cfs** |
| 5/14 | 0 | 6/9 | 13600 |
| 5/15 | 0 | 6/10 | 7800 |
| 5/16 | 0 | 6/11 | 4800 |
| 5/17 | 0 | 6/12 | 3190 |
| 5/18 | 0 | 6/13 | 2380 |
| 5/19 | 0 | 6/14 | 1840 |
| 5/20 | 0 | 6/15 | 1490 |
| 5/21 | 0 | 6/16 | 1280 |
| 5/22 | 0 | 6/17 | 1110 |
| 5/23 | 0 | 6/18 | 1000 |
| 5/24 | 0 | 6/19 | 929 |
| 5/25 | 0 | 6/20 | 856 |
| 5/26 | 0 | 6/21 | 792 |
| 5/27 | 0 | 6/22 | 745 |
| 5/28 | 0 | 6/23 | 695 |
| 5/29 | 0 | 6/24 | 647 |
| 5/30 | 1 | 6/25 | 609 |
| 5/31 | 500 | 6/26 | 603 |
| 6/1 | 2300 | 6/27 | 581 |
| 6/2 | 4600 | 6/28 | 557 |
| 6/3 | 7000 | 6/29 | 530 |
| 6/4 | 13000 | 6/30 | 503 |
| 6/5 | 25000 | 7/1 | 460 |
| 6/6 | 57900 | 7/2 | 431 |
| 6/7 | 61700 | 7/3 | 398 |
| 6/8 | 28500 | | |

Table A-8: 2008 Lower Kuparuk River discharge data. USGS station ID number 15896000. Day of peak discharge is highlighted.

| 2008 Lower Kuparuk River Discharge Data | | | | |
|---|---|---|---|---|
| **Date** | **cfs** | | **Date** | **cfs** |
| 5/13 | 0 | | 6/3 | 21000 |
| 5/14 | 0 | | 6/4 | 18600 |
| 5/15 | 0 | | 6/5 | 16200 |
| 5/16 | 0 | | 6/6 | 11000 |
| 5/17 | 0 | | 6/7 | 7460 |
| 5/18 | 0 | | 6/8 | 5280 |
| 5/19 | 0 | | 6/9 | 4110 |
| 5/20 | 0 | | 6/10 | 3200 |
| 5/21 | 0 | | 6/11 | 2560 |
| 5/22 | 0 | | 6/12 | 2130 |
| 5/23 | 0 | | 6/13 | 1870 |
| 5/24 | 0 | | 6/14 | 1680 |
| 5/25 | 10 | | 6/15 | 1500 |
| 5/26 | 40 | | 6/16 | 1330 |
| 5/27 | 200 | | 6/17 | 1190 |
| 5/28 | 700 | | 6/18 | 1070 |
| 5/29 | 4000 | | 6/19 | 991 |
| 5/30 | 9000 | | 6/20 | 947 |
| 5/31 | 30000 | | 6/21 | 1260 |
| 6/1 | 27000 | | 6/22 | 1460 |
| 6/2 | 24000 | | | |

Table A-9: 2009 Lower Kuparuk River discharge data. USGS station ID number 15896000. Day of peak discharge is highlighted.

| 2009 Lower Kuparuk River Discharge Data | | | | |
|---|---|---|---|---|
| **Date** | **cfs** | | **Date** | **cfs** |
| 5/15 | 0 | | 6/6 | 17600 |
| 5/16 | 0 | | 6/7 | 13500 |
| 5/17 | 0 | | 6/8 | 17600 |
| 5/18 | 0 | | 6/9 | 17600 |
| 5/19 | 0 | | 6/10 | 12300 |
| 5/20 | 0 | | 6/11 | 8860 |
| 5/21 | 20 | | 6/12 | 12700 |
| 5/22 | 1000 | | 6/13 | 10000 |
| 5/23 | 5000 | | 6/14 | 6660 |
| 5/24 | 12000 | | 6/15 | 4650 |
| 5/25 | 25000 | | 6/16 | 3640 |
| 5/26 | 35000 | | 6/17 | 4970 |
| 5/27 | 28000 | | 6/18 | 4570 |
| 5/28 | 22000 | | 6/19 | 3340 |
| 5/29 | 17000 | | 6/20 | 2650 |
| 5/30 | 14000 | | 6/21 | 2190 |
| 5/31 | 13000 | | 6/22 | 1830 |
| 6/1 | 15400 | | 6/23 | 1530 |
| 6/2 | 25500 | | 6/24 | 1360 |
| 6/3 | 37900 | | 6/25 | 1230 |
| 6/4 | 33500 | | 6/26 | 1160 |
| 6/5 | 23800 | | | |

Table A-10: 2010 Lower Kuparuk River discharge data. USGS station ID number 15896000. Day of peak discharge is highlighted.

| 2010 Lower Kuparuk River Discharge Data | | | |
|---|---|---|---|
| **Date** | **cfs** | **Date** | **cfs** |
| 5/18 | 0 | 6/9 | 25800 |
| 5/19 | 0 | 6/10 | 18400 |
| 5/20 | 0 | 6/11 | 12400 |
| 5/21 | 0 | 6/12 | 8020 |
| 5/22 | 0 | 6/13 | 5630 |
| 5/23 | 0 | 6/14 | 3850 |
| 5/24 | 0 | 6/15 | 2700 |
| 5/25 | 0 | 6/16 | 2050 |
| 5/26 | 0 | 6/17 | 1650 |
| 5/27 | 200 | 6/18 | 1410 |
| 5/28 | 2000 | 6/19 | 1250 |
| 5/29 | 4000 | 6/20 | 1090 |
| 5/30 | 9000 | 6/21 | 1010 |
| 5/31 | 20000 | 6/22 | 927 |
| 6/1 | 33000 | 6/23 | 843 |
| 6/2 | 30000 | 6/24 | 792 |
| 6/3 | 29000 | 6/25 | 745 |
| 6/4 | 27000 | 6/26 | 702 |
| 6/5 | 34000 | 6/27 | 658 |
| 6/6 | 36000 | 6/28 | 617 |
| 6/7 | 40000 | 6/29 | 585 |
| 6/8 | 33000 | 6/30 | 570 |

**Appendix B**

**Upper Kuparuk River Discharge Data**

Table A-11: 2005 Upper Kuparuk River discharge data. Peak discharge from first flood event is highlighted.

| 2005 Upper Kuparuk River Discharge Data | | | | |
|---|---|---|---|---|
| **Date** | **cfs** | | **Date** | **cfs** |
| 5/1 | 0 | | 6/1 | 42 |
| 5/2 | 0 | | 6/2 | 38 |
| 5/3 | 0 | | 6/3 | 41 |
| 5/4 | 0 | | 6/4 | 41 |
| 5/5 | 0 | | 6/5 | 47 |
| 5/6 | 0 | | 6/6 | 46 |
| 5/7 | 0 | | 6/7 | 43 |
| 5/8 | 0 | | 6/8 | 40 |
| 5/9 | 0 | | 6/9 | 41 |
| 5/10 | 0 | | 6/10 | 42 |
| 5/11 | 96 | | 6/11 | 45 |
| 5/12 | 314 | | 6/12 | 47 |
| 5/13 | 291 | | 6/13 | 41 |
| 5/14 | 243 | | 6/14 | 35 |
| 5/15 | 149 | | 6/15 | 32 |
| 5/16 | 68 | | 6/16 | 29 |
| 5/17 | 119 | | 6/17 | 25 |
| 5/18 | 241 | | 6/18 | 22 |
| 5/19 | 189 | | 6/19 | 19 |
| 5/20 | 170 | | 6/20 | 16 |
| 5/21 | 225 | | 6/21 | 15 |
| 5/22 | 200 | | 6/22 | 14 |
| 5/23 | 175 | | 6/23 | 12 |
| 5/24 | 155 | | 6/24 | 11 |
| 5/25 | 130 | | 6/25 | 12 |
| 5/26 | 135 | | 6/26 | 11 |
| 5/27 | 115 | | 6/27 | 8 |
| 5/28 | 95 | | 6/28 | 7 |
| 5/29 | 77 | | 6/29 | 8 |
| 5/30 | 58 | | 6/30 | 11 |
| 5/31 | 48 | | | |

Table A-12: 2006 Upper Kuparuk River discharge data. Peak discharge from first flood event is highlighted.

| 2006 Upper Kuparuk River Discharge Data | | | | |
|---|---|---|---|---|
| **Date** | **cfs** | | **Date** | **cfs** |
| 5/1 | 0 | | 6/1 | 45 |
| 5/2 | 0 | | 6/2 | 28 |
| 5/3 | 0 | | 6/3 | 18 |
| 5/4 | 0 | | 6/4 | 15 |
| 5/5 | 0 | | 6/5 | 19 |
| 5/6 | 0 | | 6/6 | 23 |
| 5/7 | 0 | | 6/7 | 42 |
| 5/8 | 0 | | 6/8 | 62 |
| 5/9 | 0 | | 6/9 | 77 |
| 5/10 | 0 | | 6/10 | 77 |
| 5/11 | 0 | | 6/11 | 69 |
| 5/12 | 0 | | 6/12 | 51 |
| 5/13 | 0 | | 6/13 | 52 |
| 5/14 | 0 | | 6/14 | 60 |
| 5/15 | 0 | | 6/15 | 275 |
| 5/16 | 57 | | 6/16 | 149 |
| 5/17 | 61 | | 6/17 | 89 |
| 5/18 | 80 | | 6/18 | 66 |
| 5/19 | 113 | | 6/19 | 82 |
| 5/20 | 191 | | 6/20 | 85 |
| 5/21 | 166 | | 6/21 | 69 |
| 5/22 | 74 | | 6/22 | 58 |
| 5/23 | 75 | | 6/23 | 88 |
| 5/24 | 94 | | 6/24 | 151 |
| 5/25 | 116 | | 6/25 | 116 |
| 5/26 | 116 | | 6/26 | 130 |
| 5/27 | 154 | | 6/27 | 226 |
| 5/28 | 148 | | 6/28 | 139 |
| 5/29 | 109 | | 6/29 | 98 |
| 5/30 | 78 | | 6/30 | 79 |
| 5/31 | 53 | | | |